DE GRUYTER DOI 10.1515/corrrev-2012-0018 — Corros Rev 2013; 31(1): 1–31

Sridhar Ramamurthy and Andrej Atrens*

Stress corrosion cracking of high-strength steels

Abstract: The mechanisms of stress corrosion cracking (SCC) and hydrogen embrittlement were recently reviewed by Lynch in this journal. The present review, in contrast, focuses on the rate-limiting step of the SCC of low-alloy high-strength steels in water and particularly focuses on the influence of the applied stress rate on the SCC of low-alloy high-strength steels. Linearly increasing stress tests of low-alloy high-strength steels in distilled water indicated that the stress corrosion crack velocity increased with increasing applied stress rate until the maximum crack velocity, corresponding to v_{II} in fracture mechanics tests in distilled water. Moreover, the crack velocity was dependent only on the applied stress rate and was not influenced by the steel composition. The rate-limiting step could be the rupture of a surface film, which would control the rate of metal dissolution and/or the production and transport of hydrogen to the crack tip or to the regions ahead of the crack tip.

Keywords: linearly increasing stress test (LIST); low-alloy high-strength steel; stress corrosion cracking.

***Corresponding author: Andrej Atrens**, Division of Materials, School of Mechanical and Mining Engineering, The University of Queensland, St. Lucia, Queensland 4072, Australia, e-mail: andrejs.atrens@uq.edu.au
Sridhar Ramamurthy and Andrej Atrens: Division of Materials, School of Mechanical and Mining Engineering, The University of Queensland, St. Lucia, Queensland 4072, Australia; and Surface Science Western, The University of Western Ontario, London, Ontario N6C 0J3, Canada

1 Introduction

Stress corrosion cracking (SCC) can occur in structures and machinery where stressed metallic parts are in contact with an environment (Dietzel, 2001; Fang et al., 2003; Warke, 2002; Winzer et al., 2005). SCC can occur at a stress intensity factor below the fracture toughness, K_{IC}, and at a stress below the yield stress. Examples include high-strength steels in sulfide solutions [sulfide cracking (Pendley, 2010; Rhodes, 2001)], mild steels in caustic solutions [caustic cracking (Nakayama, 2007; Rebak, 2006)], and Cu alloys in ammonia [season cracking (Jones, 1992)]. These well-known examples suggest a metal-environment specificity. However, Speidel (1984) suggested that SCC occurs in many environments. Nevertheless, SCC occurs under specific conditions of electrode potential, environment, and material.

SCC leads to fast fracture when the crack length combined with the applied load causes the fracture toughness to be exceeded (Gangloff, 2003; Hodge & Mogford, 1979; Kalderon, 1972; Liu & Macdonald, 1997). This reduces the useful strength of a component. Unlike crack growth due to fatigue, SCC has not been incorporated into lifetime predictions owing to the complex nature of SCC. SCC can result in catastrophic failure, such as the steam turbine at the Hinkley Point 'A' Power Plant in 1969 (Hodge & Mogford, 1979; Kalderon, 1972) and other catastrophic failures (Bennett, 1981; Gangloff, 2003). SCC in steam turbine rotors was a significant problem in the United States (Lyle & Burghard, 1982; Speidel & Bertilsson, 1984). Hence, research on the root causes of SCC was an ongoing effort (Fang et al., 2003; Villalba & Atrens, 2008a). One way of reducing SCC is to use lower-strength steels, which may not be economical. Alternatively, if the influence of the controlling parameters can be understood, it would be possible to quantify SCC crack growth. To understand the influence of various parameters, the mechanism of cracking and the rate-controlling step should be identified.

This study aimed to identify the rate-limiting step and the processes involved in SCC of low-alloy high-strength steels in water. This review follows on from the recent reviews by Lynch (2012a,b), which focused on the mechanisms of SCC and hydrogen embrittlement (HE). In contrast, the present review focuses on understanding the rate-limiting step and on the SCC of low-alloy high-strength steels. SCC of low-alloy high-strength steels exhibits a high dependence of the crack velocity on the yield strength. Speidel (1984) and Speidel and Bertilsson (1984) showed that the crack velocity increased by seven orders of magnitude for quenched and tempered steels when the yield strength was increased from 800 to 1700 MPa (Figure 1). The mechanism for this dependence is presently not known.

On the issue of the relevance of using pure water for SCC evaluations of SCC of high-strength steels, research to understand the basics of SCC is best done in the simplest environment. If SCC occurs in distilled water, it is important to understand what occurs in distilled water.

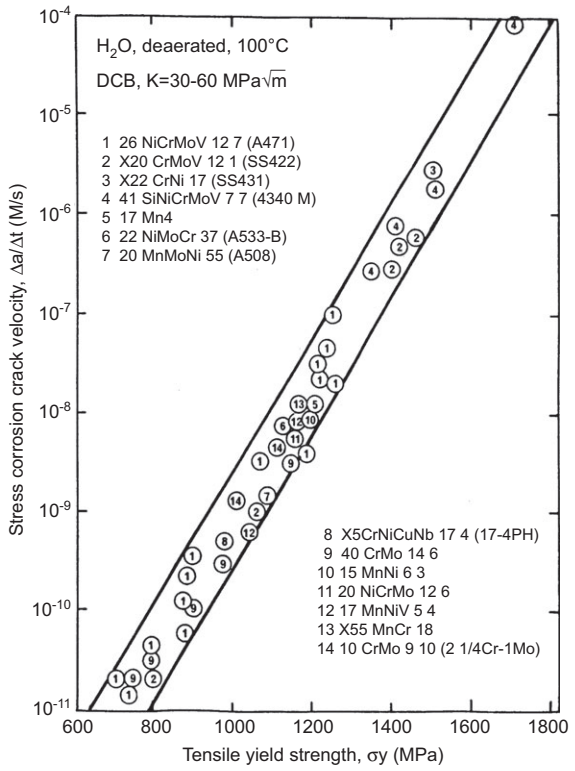

Figure 1 The relationship between the yield strength and the stress corrosion crack velocity for low-alloy high-strength quenched and tempered steels in water at 100°C. Steel composition had limited influence on crack velocity, through its influence on the yield strength. Reprinted from Speidel (1984) and Speidel and Bertilsson (1984) with permission from Springer.

It also means that special ions are not needed in the water. It means that chlorides, for example, may not be necessary to cause SCC. In a practical sense, this is also important because it is not possible to stop SCC by removing the "damaging ion" out of the solution. The water itself is part of the cause for SCC. The influence of impurities and solute is beyond the primary scope of this review

This work particularly focuses on the use of the linearly increasing stress test (LIST) (Atrens, Brosnan, Ramamurthy, Oehlert, & Smith, 1993; Atrens & Oehlert, 1998; Oehlert & Atrens, 1998; Salmond & Atrens, 1992; Wang & Atrens, 1996, 2003b, 2004; Winzer, Atrens, Dietzel, Song, & Kainer, 2008; Winzer et al., 2008) to study the influence of the applied stress rate on the SCC of low-alloy high-strength steels. LIST uses smooth tensile test specimens and can be used to study both crack initiation and crack propagation. The use of LIST to study SCC of low-alloy high-strength steels is of interest because much of the SCC research on high-strength steels has been carried out on precracked specimens. LIST can identify the parameters that control stress corrosion crack initiation. The study of the influence of the crack tip stress rate has been a neglected area and seems to offer new insights on the kinetics of SCC and possibly may help to identify the rate-limiting step.

The studies by Magdowski (1987b, 1988) and Rieck, Atrens, Ramamurthy, Gates, and Smith (1988) indicated that the SCC mechanism in this system probably varies with temperature. Thus, it is necessary to consider separately "high" and "low" temperature regimes of stress corrosion for these steels.

Furthermore, much of the experimental work in the literature dealing with SCC in high-strength steels in aqueous environments has been performed in solutions with a significant concentration of ions from a dissolved salt, an acid, or a base. Results from these tests can only be compared with those for pure water when due regard is given to possible changes in cracking induced by this modification of the cracking environment.

This study does not deal with the SCC of mild steel, maraging steel, or pipeline steels. Results from these steels are examined when no results were available from low-alloy high-strength steels. Caution needs to be exercised in drawing conclusions from such information.

SCC of high-strength steels has often been attributed to a mechanism of HE (Bath & Troiano, 1972; Brown, 1971; Eliaz, Shachar, Tal, & Eliezer, 2002; Kerns, Wang, & Staehle, 1977; Kortovich & Steigerwald, 1972; Nelson & Williams, 1977; Parkins, 1972; Sandoz, 1972), although some reviewers (Marichev & Rosenfield, 1976; Parkins, 1972) call into question the view that hydrogen is the sole mechanism. Some evidence (Magdowski, 1987b; Magdowski & Speidel, 1988) has highlighted the possibility of SCC being due to anodic dissolution (AD). Another mechanism that has been mentioned is the surface mobility mechanism, proposed by Farina, Duffo, and Galvele (2005b) and Galvele (1993). These mechanisms are discussed in Section 3. In view of the industrial importance of the field and the substantial number of recent publications aiming to clarify the operating mechanisms, it is an appropriate time to review present theories. It should be noted that whereas the mechanism of SCC in high-strength low-alloy steels in the high-strength condition is under question, the SCC of low-strength steels is generally attributed to AD (Parkins, 1972).

Low-alloy steels are normally used in the quenched and tempered condition, so a range of strengths can be produced in any steel by heat treatment. This work studied steels that have yield strength >1000 MPa, and these are considered high-strength steels.

2 Testing methods

This section reviews existing SCC test methods and their relative merits and disadvantages, which led to the development of the LIST.

2.1 Constant strain test

The specimen is subjected to a constant strain through a restraining frame, and the load relaxation in the specimen is noted as a function of time. SCC susceptibility is determined by the time to failure and the number of cracks present on the specimen surface. Results from this type of measurement need to be analyzed carefully, as the time to failure depends on the stiffness of the restraining frame and the ductility of the specimen. Hence, this test provides a qualitative measure of SCC (Yoshino, 1983). However, if the time for crack initiation can be considered as a measure of SCC susceptibility, this test has been shown to provide a reasonable measurement (Yoshino, 1983). This test could also be useful in situations where the crack initiation and failure occur within a short period of time, such as in sulfide stress cracking (Yamamoto, Ueno, Higashiyama, Sato, & Hashimoto, 1985). Hence, in many situations, this test has been used as a screening test.

2.2 Constant load test

A tensile specimen is subjected to a constant applied load, and the time to failure is measured. The time to failure includes both the time for crack initiation and the time for the crack to grow to a critical length. This test is repeated at various applied loads, and the time to failure is plotted as a function of the applied load or stress, thus defining the threshold stress (σ_{SCC}) below which stress corrosion cracks do not propagate (Figure 2). A disadvantage with this test is the long testing time required to produce a valid measurement of threshold stress. Also, the time required for crack initiation and the time for crack propagation cannot be individually estimated. Despite these drawbacks, this test method has been widely applied to study the sulfide cracking (Du, Tao, & Li, 2004), the chloride cracking (Bauernfeind, Haberl, Mori, & Falk, 2006; Jin, 1994) and the SCC of high-strength steels (Oehlert & Atrens, 1996).

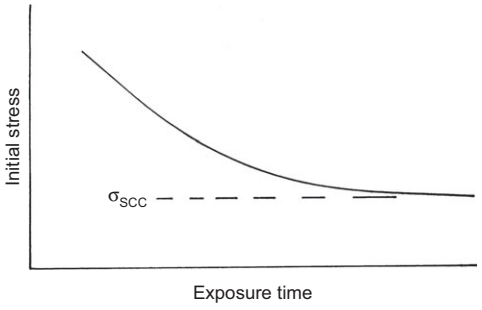

Figure 2 Schematic diagram of time to failure vs. initial applied stress from a series of constant-load SCC tests using smooth tensile specimens.

2.3 Fracture mechanics tests

Precracked fracture mechanics specimens have been widely used to study stress corrosion crack propagation. Precracking eliminates the uncertainty due to crack initiation. The stress corrosion crack velocity is plotted as a function of the stress intensity factor at the crack tip. Typical results are presented in Figure 3. SCC can be described by two parameters: K_{ISCC}, the threshold stress intensity factor for SCC; and v_{II}, the stress corrosion crack velocity in region II. v_{II} is generally independent of the stress intensity factor, although there are reports of the stress corrosion crack velocity increasing slowly with increasing stress intensity factor (Hirose & Mura, 1984; Nelson & Williams, 1977). There is some disagreement as to whether there is a true threshold for SCC, i.e., a stress intensity factor K_{ISCC} below which SCC does not occur, or whether the crack velocity is simply dependent on stress intensity factor in this region as indicated in Figure 3. It

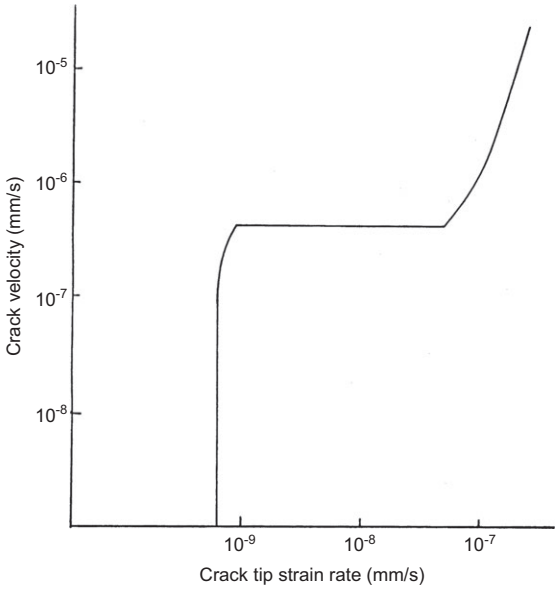

Figure 3 Schematic diagram of stress corrosion crack velocity vs. stress intensity factor (which controls crack tip strain rate) in fracture mechanics SCC tests using precracked specimens.

is possible in the low-alloy steel-water system to measure crack velocities much lower than v_{II}, suggesting that K_{ISCC} is not a true constant (Speidel, 1984) but rather has a value dependent on the crack velocity, which is regarded as insignificant. This varies between laboratories, but it is common to use 10^{-11} m/s, the lowest easily measured crack velocity, as a criterion for insignificant SCC (Andresen, Angeliu, & Young, 2001; Andresen, Young, Catlin, & Gordon, 2005; Toloczko, Andresen, & Bruemmer, 2007).

2.4 Constant extension rate test (CERT)

The slow strain rate test (SSRT) is also known as the constant extension rate test (CERT). In a CERT (Parkins, 1979a,b), a smooth tensile specimen is subjected to an applied extension rate while being exposed to the environment. The test ends with specimen failure either by ductile fracture or by SCC. The failure stress in an SCC environment can be much lower than in an inert environment. Severity of SCC is usually expressed by time to failure, reduction in ductility, reduction in the ultimate tensile strength, fracture morphology, or plastic strain to fracture.

If the applied extension rate is high, ductile fracture occurs, as there is not sufficient time for SCC. At much lower extension rates, again ductile failure may also occur due to insufficient corrosion and complete passive film formation at the crack tip. In between these two extremes of strain rates, there is SCC (Figure 4). However, in most alloy-environment systems, the SCC susceptibility increases with decreasing extension rate. These tests have been widely used in SCC research because of their short duration compared to the constant-load and constant-strain tests (ASTM, 1979). One disadvantage is that a large fraction of the test duration occurs after the initiation of stress corrosion cracks. During this stage, the duration of the test is determined by the ductility of the specimen as well as by the stress corrosion crack velocity.

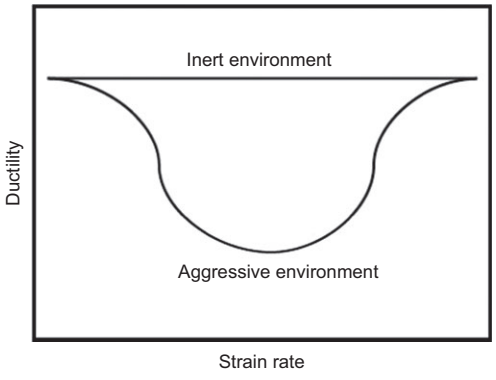

Figure 4 Schematic diagram presenting the results from SSRTs. SCC may occur at intermediate strain rates, where reduction in ductility is observed. At the two ends of this region, ductile fracture may occur in some systems. However, in many systems, ductility continues to decrease with decreasing strain rate.

2.5 Linearly increasing stress test (LIST)

To overcome these shortcomings, the LIST was developed (Atrens et al., 1993). In this LIST method, plain unnotched specimens are simultaneously exposed to an environment and subjected to an applied stress increasing linearly at a controlled rate. The LIST apparatus is based on the principle of a lever beam, as illustrated in Figure 5. One side of the lever beam is connected to the specimen, whereas the other side has a known load. Movement of the load away from the fulcrum increases the load to the specimen. The applied engineering stress is calculated from the position of the load at any time and the original area of cross section of the specimen. When the applied stress exceeds the threshold stress, σ_{th}, stress corrosion cracks initiate. When the crack length combined with the applied stress causes the fracture toughness to be exceeded, the specimen undergoes rapid fracture. This test ends with specimen facture, as in the CERT, either by SCC or by fast failure. This test is repeated at various applied stress rates, from fast to slow. SCC susceptibility can be characterized by the following: (a) threshold stress for SCC, σ_{th}; (b) comparison of the fracture stress in the environment to that in an inert environment; (c) comparison of the ductility (reduction in area or

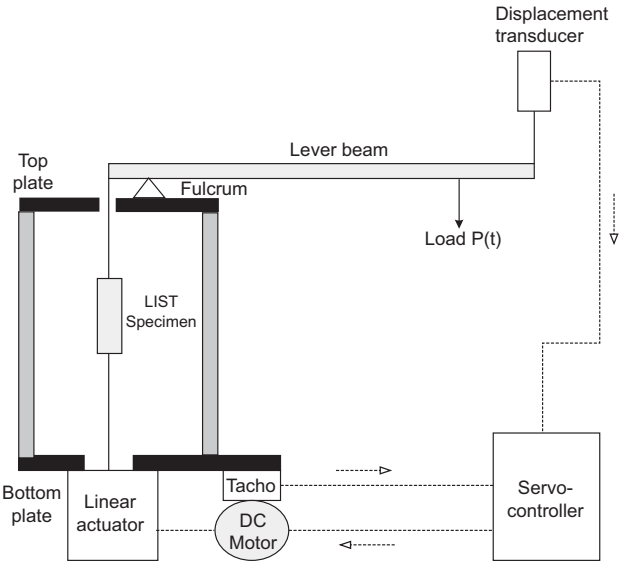

Figure 5 A schematic overview of the LIST apparatus (Atrens et al., 1993).

reduction in elongation) of the specimens in the environment and an inert environments, as stress corrosion failures are associated with little macroscopic plastic deformation during crack propagation; and (d) comparison of the fracture surfaces: intergranular SCC (IGSCC) or transgranular SCC (TGSCC) associated with low ductilities in an environment, compared to dimple fracture surfaces associated with high ductility in an inert environment. For example, the measured fracture stress at various applied stress rates in an inert environment and in an aggressive environment is plotted as a function of the applied stress rate (Figure 6). At high applied stress rates, there is insufficient time for crack propagation, giving a fracture stress similar to that in an inert environment. At lower applied stress rates, stress corrosion cracks propagate, and the specimen fails at a stress lower than in an inert environment.

This type of test should not be confused with the constant-loading rate tests performed by Coleman, Weinstein, and Rostoker (1961), in which specimens (0.25-in., 5.0 mm, diameter) were loaded at a rate of 200 lb/min (890 N/min) to some arbitrary maximum stress and immediately unloaded, removed from the test assembly, and examined for surface cracks at 20× magnification. The stress at which the cracks were just resolvable was designated as the stress corrosion fracture stress, which is in fact the stress required to open the microcracks so that they were visible at 20× and not the true fracture stress.

The LIST method offers the advantage that the strain rate on the specimen can be controlled through the applied stress rate. With the help of a potential drop technique, the threshold stress can be measured. Thus, this method combines the advantages of the constant-load tests and the constant-strain rate tests. Also, it is be quicker than either.

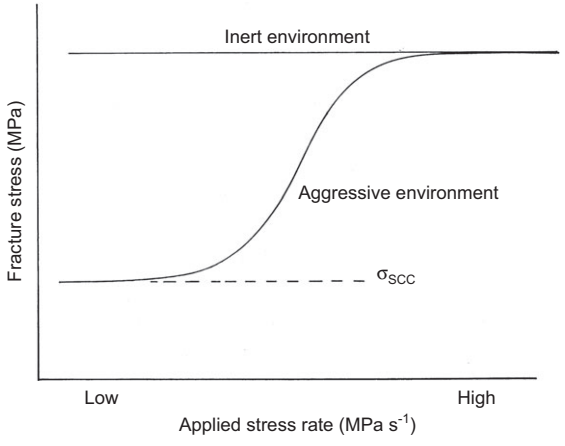

Figure 6 Schematic diagram of the results from the LIST tests. There is SCC at intermediate and low applied stress rates. The threshold stress for SCC may level off at low applied stress rates.

This test was originally developed to study the SCC behavior of high-strength steel in water (Atrens et al., 1993; Ramamurthy & Atrens, 1993, 2010; Ramamurthy, Lau, & Atrens, 2011). Since then, this test has been employed to study the SCC behavior of rock bolts (Gamboa & Atrens, 2003a,b, 2005; Villalba & Atrens, 2007, 2008b), commercial steels (Liu, Irwanto, & Atrens, 2013; Villalba & Atrens, 2008a), SCC and creep behavior of Aermet 100 (Oehlert & Atrens, 1998), copper alloys (Salmond & Atrens, 1992), magnesium (Atrens, Winzer, Song, Dietzel, & Blawert, 2006; Jia, Song, & Atrens, 2007; Winzer, Atrens, Dietzel, Song, et al., 2008; Winzer Atrens, Dietzel, Song, & Kainer, 2007), and X65 pipeline steel (Wang & Atrens, 1996, 2003b).

3 SCC mechanisms

3.1 Introduction

If SCC involves electrochemical processes and is controlled by the electrochemical conditions at the crack tip (Turnbull, 1992, 1993), then it is important to understand the electrochemical potential, pH, ion concentrations, and reactions occurring at the crack tip. For low-alloy steels in water, it is difficult to define the conditions at the crack tip because of the high resistivity of water. However, at the free corrosion potential, the rate of the anodic reaction equals the rate of the cathodic reaction. The electrochemical reactions most likely to occur at the crack tip in low-alloy steels in water are:

Anode

$$M \rightarrow M^{n+} + ne^- \quad (1)$$

Cathode

$$O_2 + 2H_2O + 4e^- \rightarrow 4OH^- \quad (2)$$

$$2H^+ + 2e^- \rightarrow H_2 \quad (3)$$

Which of the two cathodic reactions occurs depends on the local electrochemical conditions at the crack tip, such as potential, solution pH, and supply of oxygen, and may be critical in determining which of the two mechanisms of SCC (HE or AD) is operable.

3.2 Anodic dissolution (AD)

In the AD mechanism of SCC, the crack advance is due to the AD reaction at the crack tip. The crack sides are

assumed to be covered with a passive film, which inhibits corrosion and maintains the high aspect ratio necessary for a stress corrosion crack (Parkins, 1974; Vermilyea & Diegle, 1976). For SCC by AD, corrosion at the crack tip is a necessary but not a sufficient condition. The likelihood of corrosion in the crack can be assessed by referring to a Pourbaix diagram if the crack tip conditions are known. This also allows assessment of the possibility of passive film formation. In practice, it is difficult to determine the pH and potential at the crack tip. The crack velocity produced by an AD mechanism is directly related to the rate of metal dissolution at the crack tip (Dix, 1940). This suggests the possibility of comparing crack growth rates with the rate of metal dissolution as measured on film-free surfaces. This comparison presents some difficulties, however. Quenched and tempered steels in water tend to crack along grain boundaries (GBs) where segregation of impurities may alter the metal composition, so dissolution rates from metal of bulk composition may not be applicable. There is also, in the case of SCC, the possibility of strain-assisted dissolution, a factor again not present in dissolution of a smooth surface.

The slip dissolution model was proposed as a refinement to the AD model (Hoar & West, 1962; Newman, 1981; Scully, 1972a,b; Staehle, 1972; Vermilyea, 1972). In this model, the passive film forms over the crack sides and the crack tip. This results in the crack growth being stopped until the buildup of the crack tip strain is sufficient to rupture the crack tip passive film. The crack tip advances intermittently when the crack tip is exposed to the test solution. The crack velocity is influenced by the extent of crack growth at each step as well as the interval between two rupture events.

Some details of the processes are open to question. For example, the passive film may be fractured in a brittle manner, leaving the metal surface completely bare, or the film may be ductile, so that it is simply thinned by the strain (Diegle & Vermilyea, 1976; Vermilyea & Diegle, 1976). In order to overcome this drawback, Diegle and Vermilyea (1976) and Vermilyea and Diegle (1976) assumed that no plastic deformation occurs during the dissolution process, but that creep processes, after the AD, control the plastic deformation. Hall (2008, 2009) noted the similarities between the slip dissolution model and high-temperature creep crack growth and also proposed a revised model incorporating the role of creep in the slip dissolution model. His model also takes into account the rate of loading on the film rupture/dissolution/repassivation cycle occurring at the crack tip. Another complication arising from the slip dissolution model is the possibility that, when the passive film ruptures in a brittle manner, the crack may propagate in a brittle manner for some distance into the (otherwise ductile) metal ahead of the crack (Sieradzki & Newman, 1986). Sieradzki and Newman (1986) also suggested that the large depth of corrosion at each film rupture cycle, influenced by the plastic strain distribution ahead of the crack, would exceed the mechanical crack tip opening and would be inconsistent with the observed crack geometry and relatively little corrosion observed on the fracture surface. They concluded that the slip dissolution model aided by intergranular corrosion could explain IGSCC, but ruled out this model for the TGSCC.

3.3 Hydrogen embrittlement (HE)

Subcritical cracking of steels in H_2/H_2S atmospheres is the basis for the HE mechanisms (Nelson & Williams, 1977; Simmons, Pao, & Wei, 1978; Thompson, & Bernstein, 1981). Hydrogen may cause embrittlement as a result of hydrogen being present within the alloy during loading (internal HE) or the alloy under load exposed to a hydrogen-containing environment (external HE) (Eliaz et al., 2002). This results in reduced ductility, reduced strength, and nonductile fracture.

For HE to occur, there must be a source of hydrogen, the hydrogen must be transported to the location where embrittlement occurs by some transportation processes, and a mechanism needs to cause embrittlement at the failure location. In water and other aqueous solutions, with the absence of external hydrogen, the source of hydrogen for HE is the cathodic reaction, and the occurrence of this reaction is a necessary condition for any HE mechanism of SCC. If the crack tip electrochemical conditions are known, the likelihood of reaction 3 can be assessed by reference to the respective Pourbaix diagram. For HE to occur, the hydrogen concentrations need not be close to the solid solubility limit. Even low concentrations of hydrogen can cause HE. The concentration required for HE is also influenced by the yield strength; steel susceptibility increases with increasing yield strength. For example, a few parts per million of hydrogen was found to cause HE in high-chromium martensitic steels over a large temperature range (-130°C to 250°C) (Beghini, Benamati, & Bertini, 1996). Steel composition is also known to influence HE by modifying hydrogen absorption characteristics (Buckley, Placzankis, Lowder, Brown, & Brown, 1991; Jung, 1996; Liou, Shieh, Wei, & Wang, 1993; Rieck, 1985; Rieck et al., 1988). For example, alloying elements and impurities can influence the corrosion potential of the steel, thereby changing the interaction of the steel with

hydrogen, can act as traps for hydrogen, can poison the GBs, and can form passive films and protective surface layers.

Transportation of hydrogen to the degradation site is an important step in the HE process. Diffusion of hydrogen, the incubation period, and the hydrogen concentration buildup are important features that reflect the transportation kinetics (Birnbaum, 1994; Birnbaum & Sofronis, 1994). Introduction of the hydrogen atom (from solution in the case of SCC in water) into the lattice results in localized volume (Peisl, 1978) and modulus changes (Mazzolai & Birnbaum, 1985; Mazzolai & Lewis, 1985). As a result, there is diffusion through normal interstitial lattice sites (NILSs) toward these regions to eliminate the chemical potential gradient. Hydrogen transported through NILS diffusion can accumulate at various microstructural heterogeneities, such as dislocations, GBs, inclusions, voids, and impurity atoms (Gibala & DeMiglio, 1981; Wert, 1983). Trapping has been observed to be an important part of HE, and its significance lies in the embrittling mechanism (Gibala & DeMiglio, 1981; Stevens & Bernstein, 1985). From the experimental data on annealed iron, Oriani and Josephic (1980) concluded that interfaces and microcracks were involved in trapping hydrogen. On the basis of the data from iron, Kumnick and Johnson (1974) estimated a trap density of 2.77×10^{22} traps/m^2 and concluded that this trap density is not likely to be associated with the long-range elastic-stress fields of dislocations. On the basis of later work (Johnson & Lin, 1981), they concluded that the trap binding energy is independent of temperature and the amount of plastic deformation, and that the traps could be associated with imperfections, point defects, and dislocation debris. Hirth (1980) observed that that the trap binding energy reported by Kumnick and Johnson (1980) could correspond to the trap sites of standard mixed or screw dislocation cores.

Hydrogen transport by dislocations toward the crack tip may also be important (Tien, Nair, & Jensen, 1981). However, more dislocations also move away from the crack tip, thus cancelling the effect of hydrogen transport through dislocations. Moreover, other experimental evidence does not support hydrogen transport by dislocations (Frankel & Latanision, 1986; Ladna & Birnbaum, 1987).

Several possible mechanisms have been proposed for the embrittlement of metals by trapped hydrogen. These include (1) high gas pressure in internal voids (Zapffe & Sims, 1940), (2) hydrogen-enhanced localized plasticity (HELP) (Beachem, 1972; Birnbaum, 1994; Lynch, 1979), (3) hydrogen enhanced decohesion (HEDE) at or ahead of the crack tip (Oriani, 1970, 1978; Oriani & Josephic, 1977; Troiano, 1960), (4) reduction in surface energy by adsorption (Petch, 1956), and (5) formation of a brittle hydride and cleavage fracture (Grossbeck & Birnbaum, 1977; Lufrano, Sofronis, & Birnbaum, 1998; Westlake, 1969). Of these, HELP and HEDE appear to be viable for the SCC of high-strength steels. Formation of hydrides and the associated brittle fracture has been shown to be applicable to systems where hydrides are stable or can be stabilized by an applied stress field, such as Ti (Frandsen, Paton, & Marcus, 1973; Shih, Robertson, & Birnbaum, 1988) and Zr (Dutton, Nuttall, Puls, & Simpson, 1977). Thermodynamic calculations (Flanagan & Mason, 1981) and microscopy observations (Takano & Suzuki, 1974) tend to support the presence of hydrides causing cracking in these materials. Where conditions are not suitable for the formation and the stability of hydrides, the HELP and HEDE mechanisms have been proposed for the embrittlement process. The HELP mechanism is based on the experimental observations that over a range of temperatures and strain rates, the presence of hydrogen in a solid solution decreases the barriers to the dislocation motion. This results in an increased amount of deformation in a localized region adjacent to the fracture surface (Lynch, 2003: Robertson & Birnbaum, 1986; Rozenak, 1990). Thus, the fracture process is a highly localized plastic failure, even though the fracture is macroscopically brittle. Microscopic observations support the onset of localized plasticity and the reduced macroscopic ductility. The other viable embrittlement process is HEDE, in which the atomic bonding is weakened by the presence of hydrogen in the solid solution (Gerberich, Chen, & St. John, 1975; Oriani, 1970, 1978; Oriani & Josephic, 1977; Troiano, 1960). There is support for this mechanism from systems in which significant hydride formation does not occur, and there is also absence of significant plastic deformation in the system. Further support has been provided by a thermodynamic argument (Hirth, 1980a,b; Hirth & Rice, 1980) and chemical potential calculations (Daw & Baskes, 1984).

3.4 Surface mobility

Bianchi and Galvele (1987) and Galvele (1986, 1993) proposed the surface mobility mechanism to address some of the deficiencies in the AD and HE mechanisms. While proposing this mechanism, Galvele takes into consideration three aspects of stress corrosion cracks, namely, (1) the crack aspect ratio, the ratio between the crack length and crack opening can be well above 100, and in some cases even above 1000. This means that when the crack is propagating, the sides of the crack are expected to show

neither corrosion nor plastic deformation; (2) walls of the crack show no stress, whereas a high-stress concentration is found at the crack tip (thus, the environment is in contact with a strongly heterogeneous material over a short distance), and (3) the tensile stresses at the crack tip. In ductile materials, the stress at the crack tip increases up to the yield point, leading to a plastic zone in front of the crack. The size of the plastic zone is a function of the applied stress and the geometry of the sample.

The surface mobility mechanism postulates that SCC occurs at a temperature below 0.5 T_m, where T_m is the absolute melting point of the material. This enables volume diffusion to be ignored. It is postulated that only elastic tensile stresses are relevant to this mechanism. Significant stresses exist at the crack tip, and a tensile stress is known to reduce the free-energy formation of vacancies (Hirth & Nix, 1985). The surface mobility mechanism assumes that because of the action of the environment, only the first atomic layers of the metal are susceptible to measureable movement. Crack propagates an atomic distance every time the stressed lattice at the tip of the crack captures a vacancy. This results in a surface depletion of vacancies. The rate-controlling process is the diffusion of the vacancies along the surface.

Galvele and coworkers have shown a correlation between the predictions from this mechanism and SCC in various systems, such as embrittlement of high-purity copper in CuCl at 200°C (Bianchi & Galvele, 1987), SCC of Ag-Pd and Ag-Au alloys (Duffo & Galvele, 1988, 1990), SCC of silver alloys in bromine vapor (Bianchi & Galvele, 1994), SCC of zirconium alloys and other close packed metals and alloys (Farina & Duffo, 2004; Farina, Duffo, & Galvele, 2003; Farina, Duffó, & Galvele, 2005a), nuclear materials (Galvele, 1996), and SCC of Ag-Cd alloys in halide solutions (Duffo & Galvele, 1990).

Despite the correlations from the predictions of this mechanism, there have been some criticisms. Sieradzki and Friedersdorf (1994) observed that in one of the manifestations of this mechanism the effect of the environment is to react with the metal to produce a low-melting-point compound. They contend that the surface of a crack is a free surface, i.e., no normal stresses act on them, and that the analysis employed by Galvele for the equilibrium vacancy concentration was inappropriate. They also contend that Galvele neglected the effect of capillary process. Based on their analysis, they conclude that SCC crack propagation via surface mobility can be applicable in cases where there is a low crack-propagation rate, but that other models of cracking (AD, film-induced cleavage, etc.) should be considered for intrinsically ductile face-centered cubic metals.

Galvele (1994), in his reply, indicated that cracks can grow under compressive stress in certain alloy-environment systems and that the formation of corrosion products (oxides and other compounds) as a result of the interaction between the metal and the environment would overcome any possible effect of surface tension. He has also pointed out the alloy-environment systems where SCC can be explained by the surface mobility mechanism as a validation of his postulations.

The validity of the surface mobility mechanism was also raised by Gutman (2003). The comments made in his paper were addressed by Galvele (2003). Galvele also states that the surface mobility mechanism is applicable to only a limited number of alloy-environment systems. Additional support was provided by Vogt and Speidel (1998).

4 Strain and strain rate

4.1 Role of crack tip strain rate in SCC

For the SCC of high-strength steels in aqueous solutions, both AD and HE models require the rupture of passive films for the subsequent crack advance. For the AD model, Scully (1967, 1972a,b, 1980) proposed that (i) crack propagation would stop if the crack tip strain rate falls below the repassivation rate, and (ii) a crack tip strain rate greater than the repassivation rate leads to some other form of corrosion and not stress corrosion crack propagation. In his model, crack propagation occurs only when the crack tip strain rate is equal to the repassivation rate. Diegle and Vermilyea (1976) and Vermilyea (1972, 1976) proposed a variation of this model, in which corrosion occurs when the crack tip was bare, and this is followed by the repassivation of the crack tip. Because of the removal of some material near the crack tip from the previous corrosion process, the material just ahead of the crack tip experiences a strain transient. When the accumulated strain transient ("creep strain") reaches the critical strain required to rupture the passive film, corrosion occurs at the crack tip, resulting in crack advancement. Crack advance occurs by a cycle of film rupture and repassivation. The critical strain rate controls the frequency of film rupture events and controls the stress corrosion crack growth rate. Thus, it was proposed that the threshold intensity of SCC, K_{ISCC}, corresponds to the value of the critical crack tip strain rate (Scully, 1975). Moreover, because of the time dependency of the film rupture/repassivation events, this process is analogous to creep despite

occurring at relatively low temperatures (Vermilyea, 1972). The relationship between the repassivation rate and the film rupture rate has been schematically described by Newman (1981) in Figure 7. The threshold stress intensity factor (K_{ISCC}) is defined as the stress intensity factor below which crack growth effectively ceases. Newman has shown that decreasing K increases the degree of passivation between film rupture events, and at a value below K_{ISCC} this leads to crack arrest. Thus, K_{ISCC} may also be defined by the combination of crack tip strain rate and repassivation rate, and this definition is similar to that employed by Scully (1978, 1980).

The crack tip strain rate has also a significant role in the HE mechanism. Its first role is the generation of hydrogen during the film rupture process. Thus, the frequency of film rupture and the subsequent repassivation process influences the generation of hydrogen at the crack tip and its entry into the region ahead of the crack tip. De Moraes, Bastian, and Ponciano (2005) have shown that plastic straining of pipeline steels in low H_2S environment increased the uptake of hydrogen. They considered that this could be due to the effect of hydrogen trapping and transport promoted by moving dislocations. This is also supported by observations of Tien, Thompson, Bernstein, and Richards (1976), according to whom the transport of hydrogen promoted by moving dislocations can be four orders of magnitude higher than the hydrogen flux due to ordinary diffusion. Further support was provided in the review of Louthan, McNitt, and Sisson (1981), who showed that plastic deformation during exposure to hydrogen increased the apparent hydrogen diffusivity.

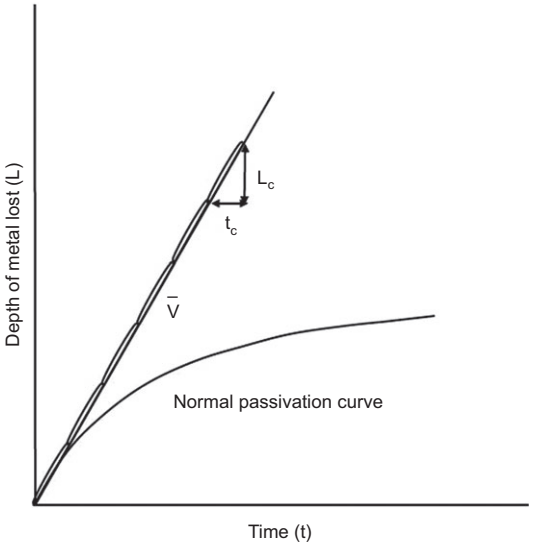

Figure 7 Schematic diagram illustrating how the mean crack velocity is influenced by the metal loss as a function of time. Reprinted from Newman (1981) with permission from Elsevier.

Tien et al. (1976) also proposed a kinetic model of hydrogen transport involving large supersaturations of hydrogen at voids and interfaces in the metal. However, Johnson and Hirth (1976) have since shown that such supersaturations are not possible in steels owing to the high diffusivity of hydrogen in the body-centered cubic α iron lattice. Transport of hydrogen by dislocations has also been proposed by Lynch (1979, 2007) and Oriani (1978). Lynch (2007) also proposed that the strain rate may influence HE mechanisms of SCC through enhanced transport of hydrogen as Cottrell atmospheres around mobile dislocations. However, contradicting evidence has been presented by Zakroczymski and Szklarska-Smialowska (1985), who found that the dislocation motion associated with plastic strain does not enhance the transport of hydrogen in iron.

The previous discussions indicate that the crack tip strain rate can act as a rate-limiting step in the kinetics of SCC. For example, in the AD model, the crack tip strain rate controls the film rupture events, thus controlling the metal dissolution rate. In the HE model, the crack tip strain rate controls the hydrogen production in some systems and its transport to locations ahead of the crack tip. For the embrittlement models involving localized plasticity, crack tip strain rate also enhanced localized plasticity through increased hydrogen productions and/or transport. Because the production of hydrogen is through the corrosion at the crack tip in aqueous solutions, the investigations into the effect of crack tip strain rate may not reveal the mechanism of SCC but may help identify the processes important in defining K_{ISCC}, the threshold stress (σ_{SCC}), and the rate-limiting step.

4.2 Experimental observations on strain rate

For the tests involving smooth specimens, the crack tip strain rate is normally controlled by the externally applied extension rate (CERT) or by the strain rate (SSRT), applied stress rate (LIST) or by the applied stress or stress intensity factor (constant-load type tests). These tests, in addition to those using precracked specimens, have been used to study the effect of crack tip strain rate on the SCC kinetics.

Maeng, Lee, and Kim (2005) employed CERT tests to study the effect of strain rate for the SCC testing of 3.5NiCrMoV steels (675 MPa yield strength) in high-temperature (50–200°C) water. They have shown that the elongation increased linearly with the logarithmic increase in the strain rate. Fracture surface morphology indicated

little deformation at low strain rates and extensive deformation at high strain rates, consistent with the observations from elongation measurements. They explained their results based on the AD mechanism: At intermediate strain rates the metal dissolution rate increased with decreasing strain rate due to greater time available for the crack tip to be present in the active condition. At higher strain rates, there was not time for sufficient metal dissolution for crack advancement and hence ductile fracture was observed in their study. At low strain rates, they considered the plastic deformation to be too low to cause film rupture and metal dissolution.

Maiya (1987) and Maiya and Shack (1984) also employed CERT tests to study the influence of crack tip strain rate on SCC of stainless steels in water. They also developed a model for crack growth based on the slip dissolution model from Ford (1982, 1984). Their data indicated that the time to failure decreased with increased strain rate for both IGSCC and TGSCC modes of failure. In converse, the crack growth rates increased with increasing applied strain rates for the measurements in a sulfate environment. The average crack tip strain rates, calculated from their model, were also found to result in increasing crack growth rates, similar to the trends observed for the applied strain rate.

Wang and Atrens (1996) also demonstrated the influence of crack tip strain rate by conducting LIST tests on a low-strength X65C pipeline steel in 1 N Na_2CO_3+1 N $NaHCO_3$ solution at 70°C. In their study, the applied strain rate was controlled by varying the applied stress rate. They found that the crack initiation stress decreased with decreasing applied stress rate. Their results were also attributed to the AD mechanism in which there is a competition between the film rupture rate (through the buildup of crack tip strain) and the repassivation rate. At higher strain rates, ductile fracture was observed due to insufficient time for corrosion processes, and the repassivation rate was critical at lower applied stress rates. Their results were found to be in the latter regime.

One of the more definitive experiments on the influence of crack tip strain rate was performed by Parkins (1979a, 1990) on a low-strength C-Mn pipeline steel loaded as cantilevers while exposed to the carbonate-bicarbonate solution at 75°C that causes IGSCC at the potential range of -600 to -700 mV_{sce}. In the experimental setup, measurement of the deflection of the beam as a function of time represented the crack tip opening displacement as a function of time, i.e., the creep and cracking response. The data are shown in Figure 8. When the potential was in the cracking range, the beam deflection response was as shown in curve A. The initial part of the curve represents

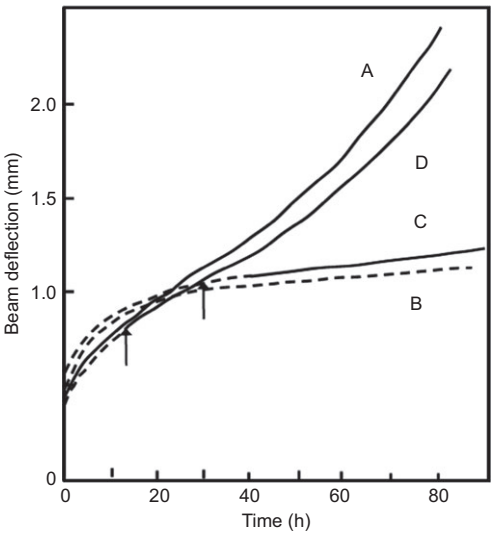

Figure 8 Beam deflection-time curves for constant-load cantilever beam tests on a pipeline steel in 1 N Na_2CO_3+1 N $NaHCO_3$ at 75°C and the effects of cracking (-0.65V_{sce}) and noncracking (-0.9 V_{sce}) potentials. Reprinted from Parkins (1979, 1990) with permission from NACE.

the creep in the plastic zone. Stress corrosion crack initiation and growth resulted in an increase in stress and further creep so that the beam deflection began to accelerate under the joint action of stress and the creep at the crack tip. In contrast, if the sample was held under the same stress intensity factor, however, at a potential where SCC did not occur, the beam deflection behavior represented the simple creep influence and was not complicated by the crack initiation and propagation effects. This was represented by the curve B in Figure 8. Thus, a difference between the two curves represented the SCC behavior of this steel in this solution. In addition to these two measurements, Parkins performed additional experiments in which the potential was held outside the SCC range (-950 mV_{sce}) for a while before switching to the susceptible potential range (-650 mV_{sce}) and vice versa. The response from these measurements is shown in curves C and D. Curve C represented the case where the potential was held outside the range for 40 h and then switched over to the susceptible range. This curve was similar to the curve B and indicated that SCC did not occur on this sample. This was despite the fact that the stress intensity factor was the same as that for the experiment shown by curve A. Parkins explained this by arguing that by the time the potential was switched over to the susceptible range, the creep rate had diminished to a value below which it could not initiate or sustain cracking. He tested this hypothesis by conducting another experiment in which the potential was at the nonsusceptible region when the experiment

Table 1 Effect of prior creep on SCC, after Rieck et al. (1988, 1989).

Specimen	Metal	Creep time (h)	Environment	Cracking	Comment
1	3.5NiCrMoV	0	H_2O	Yes	V=1.14×10^{-7} m s^{-1} at 25°C
2	3.5NiCrMoV	72	Silica gel-dried air	No	

started and switched over to the susceptible range before the creep rate had fallen to a low value, shown in curve C. Curve D represented the case in which the beam deflection behavior was similar to curve A, i.e., as if the potential switch did not matter. These results indicated that the controlling factor in the stress corrosion experiments was not the initial stress or stress intensity factor, but the creep or the strain rate at the crack tip.

Rieck and coworkers (Rieck, 1985; Rieck et al., 1988; Rieck, Atrens, & Smith, 1989) performed similar tests on quenched and tempered low-alloy high-strength steels, using precracked fracture mechanics specimens. Their results are shown in Table 1. Specimen 1 exhibited SCC, with the region II crack velocity equal to 1.14×10^{-7} m s^{-1}. In contrast, the second specimen was allowed to creep for 72 h before hot water was added, and this specimen did not exhibit cracking. Moreover, unlike Parkins, Rieck et al. did not find a minimum time of prior creep required to prevent SCC, even though the creep time was as low as 10 min in one case. They postulated that the primary creep was exhausted more rapidly in the high-strength steels employed in their study compared to the low-strength steels studied by Parkins.

In further tests, Rieck and coworkers demonstrated that it was possible to arrest a growing crack by removing the water from the cell while the specimens were still loaded and allowing creep to occur. Their results are presented in Table 2. Specimen 3 exhibited SCC when exposed to water, and the crack velocity was greater than that observed for 3.5NiCrMoV steel shown in Table 2. This is due to the greater yield strength of this material. However, when the specimen (specimen 5) was allowed to creep for 48 h in air (dried with P_2O_5) subsequent addition of water did not cause SCC on this sample. These results were again consistent with the mechanism that once primary creep was exhausted, the critical crack tip strain rate was not reached and SCC did not proceed.

Rieck and coworkers also investigated the possibility of restarting SCC once it had been arrested by creep. They found that an increase in the applied stress intensity from 20 to 65 MPa √m was required to restart cracking. These results for subcritical cracking in aqueous solutions are to be compared with behavior in pure gaseous hydrogen, where the cracking is not expected to be dependent on the crack tip strain, as hydrogen is always present and there is no passive film at the crack tip (provided the hydrogen is sufficiently pure and that the crack is started in the high-purity hydrogen atmosphere). Oriani and Josephic (1974) loaded specimens of AISI 4340 to a desired stress intensity factor and then increased the pressure of hydrogen until cracking began. The threshold stress intensity factor for cracking, K_{IH}, was found to be independent of the time for which the specimen was loaded prior to introduction of the hydrogen, for holding times between 15 min and 16 h. The results of Rieck and coworkers (Rieck, 1985; Rieck et al., 1988), however, show that for such high-strength steels, primary creep is exhausted within 10 min, so no effect would be expected within this range of holding times. Oriani and Josephic (1974) did not test specimens where the hydrogen was introduced before loading, so it is not possible to determine from their results whether prior creep has any effect on K_{IH}. The expectation that the crack tip strain is not necessary for cracking in hydrogen is partially supported by the results of Rieck and coworkers (Rieck, 1985; Rieck et al., 1988), who found that SCC, arrested by a period of creep, could be restarted by hydrogen charging. Under conditions of hydrogen charging, a dissolution reaction within the crack is not required to maintain the hydrogen supply. Because the specimen was in water, there was a passive film to be contended with, and indeed in some cases it was found necessary to abrade the side of the specimen in order to allow entry of hydrogen. In gaseous hydrogen, however, K_{IH} is expected to be an equilibrium quantity, dependent only on the hydrogen

Table 2 Effect of environment of creep inhibiting SCC, after Rieck et al. (1988, 1989).

Specimen	Metal	Creep time (h)	Environment	Cracking	Comment
3	4340	0	H_2O	Yes	V=8×10^{-5} m s^{-1}
5	4340	48	P_2O_5-dried air	No	

pressure, P_{H2}. Further experiments, with hydrogen introduced prior to loading, are required in order to determine conclusively whether crack tip strain rate affects K_{IH}.

Oehlert and Atrens (1994) investigated the room-temperature creep behavior of three high-strength steels. Parameters such as creep stress, loading rate, stress history, and heat treatment were altered, and their influence on the low-temperature creep was reported. The primary creep in all three alloys agreed well with the logarithmic creep law, and the creep mechanism was identified as pure dislocation creep. Higher stresses and high loading rates led to increased creep strains and strain rates. Reloading after a period of creep resulted in significantly decreased creep strains, and no recovery of the time-dependent deformation could be detected. The yield strength of the materials per se had no influence on the room-temperature creep, whereas the same material with decreased 0.2% offset strength showed significantly reduced time-dependent deformation. The possible interaction between primary creep and SCC was discussed.

Kinaev, Cousens, and Atrens (1999) studied the influence of hydrogen and water vapor environments on the plastic behavior in the vicinity of the crack tip for AISI 4340. Hydrogen and water vapor (at a pressure of 15 torr) significantly increased the crack tip opening displacement. The crack tip strain distribution in 15 torr hydrogen was significantly different to that measured in vacuum. In the presence of sufficient hydrogen, the plastic zone was larger and was elongated in the direction of crack propagation; moreover, there was significant creep. These observations support the hydrogen-enhanced localized plasticity model for HE in this steel. The strain distribution in the presence of water vapor also suggests that SCC in AISI 4340 occurs via the hydrogen-enhanced localized plasticity mechanism.

4.3 Influence of surface strain

Atrens and Wang (1998) studied the SCC initiation process for 4340 high-strength steel in distilled water at room temperature using an environmental scanning electron microscope. It was found that the applied stress accelerated oxide film formation, which has an important influence on the subsequent SCC initiation. SCC was observed to initiate in the following circumstances: (1) cracking of a thick oxide film, leading to SCC initiation along metal GBs; (2) the initiation of pits initiating SCC in the metal; and (3) SCC initiating from the edge of the specimen.

All these three SCC initiation circumstances are consistent with the following model, which couples SCC initiation with cracking of a surface protective oxide. There is a dynamic interaction between oxide formation, the applied stress, oxide cracking, pitting, and the initiation of SCC. An aspect of the dynamic interaction is formation of cracks in a protective surface oxide because of the applied stress, exposure to the water bare metal at the oxide crack tip, and oxidation of the bare metal, causing crack healing. Oxide crack healing would be competing with the initiation of IGSCC if an oxide crack meets the metal surface at a GB. If the IGSCC penetration is sufficiently fast along the metal GB, then the crack yaws open, preventing healing of the oxide crack. If IGSCC penetration is not sufficiently fast, then the oxidation process could produce sufficient oxide to fill both the stress corrosion crack and the oxide crack; in this case, there would be initiation of SCC but only limited propagation of SCC. Stress-induced cracks in thin oxide can induce pits, which initiate SCC, and under some conditions such stress-induced cracks in a thin oxide can directly initiate SCC.

4.4 Discussion on strain and strain rate

The above results, and in particular the observed influence of prior creep on K_{ISCC}, demonstrate that crack tip strain is critical in the SCC of high-strength steels in water. The role of crack tip strain for tests in aqueous solutions is best explained in terms of the fracture of surface films at the crack tip in order to allow a dissolution reaction to proceed. Then, K_{ISCC} can be defined as the stress intensity factor required to produce a critical crack tip strain rate, which is required to continuously rupture the surface film.

Some of the experimental data presented in the previous section, such as that of Maeng Lee, and Kim (2005) and Wang and Atrens (1996), can be explained on the basis of the AD model. Moreover, Parkins has also shown that the AD model can be applicable to the SCC of low-strength pipeline steel (Parkins, Belhimer, & Blanchard, 1993). Some of the experimental results from the high-strength steels, especially that of Rieck (1985) and Rieck et al. (1988), are explicable in terms of both AD and HE models of SCC in water, as both models require a dissolution reaction within the crack, and crack tip strain provides the means whereby this dissolution reaction can be maintained. Thus, the mechanism of SCC cannot be distinguished from such studies. Moreover, the results are useful in that they can identify the rate-controlling step of SCC in this system and have also identified a major controlling process for the SCC of steels in water, one that defines K_{ISCC}.

The film at the crack tip for 4340 may not be a passive film in the same sense as that for stainless steels. Its role, as postulated above, is to be at least partially protective (i.e., decrease the corrosion reaction) and to hinder hydrogen entry into the metal.

5 Crack velocity

5.1 Introduction

Previous sections described the evidence that the crack tip strain rate was the controlling parameter of SCC of high-strength low-alloy steels in aqueous environments. The crack tip strain rate was shown to be the rate-limiting step of SCC in this system due to the dissolution of the passive film at the crack tip, thus enabling crack advance through metal dissolution (AD mechanism) or hydrogen generation (HE mechanism). Thus, the threshold stress (σ_{SCC}) or the threshold stress intensity factor (K_{ISCC}) is defined by the minimum crack tip strain rate required to sustain crack advance and to maintain the crack aspect ratio at the crack tip. Another parameter that defines the kinetics of SCC is the crack velocity v, which controls the rate of crack propagation and the time to failure in tests using tensile specimens, such as CERT, SSRT, and LIST. Determination of crack velocity is simpler in fracture mechanics tests, which employ precracked specimens, thus eliminating the issues associated with crack initiation. Hence, these tests have been employed extensively to determine the effect of various parameters on the crack growth rate (crack velocity).

The threshold stress or the threshold stress intensity factor can also be defined as the value at which the lowest crack velocity can be measured in SCC tests. Depending on the experimental conditions, this value can be as high as 10^{-8} m s^{-1} (Simmons et al., 1978) or as low as 10^{-11} m s^{-1} (Speidel, 1984; Speidel & Magdowski, 1986). For SCC experiments in aqueous solutions, the rate-limiting step that controls the lowest crack velocity would be the critical crack tip strain rate that would be needed to maintain a balance between the rupture rate and the repassivation rate (Scully, 1967, 1980, 1972a,b), thus enabling the metal dissolution or hydrogen generation or vacancy generation at the crack tip depending on the mechanism of SCC.

As the stress/stress intensity factor is increased, the crack velocity increases until it reaches a plateau above which further increase in the stress intensity does not result in the increase in crack velocity. This is known as the plateau crack velocity, v_{II}. The rate-limiting step that controls the plateau crack velocity is dependent on the mechanism of cracking. For the AD mechanism, the maximum dissolution rate that is allowed at the bare crack tip controls the plateau crack velocity. For the HE mechanism, the rate of hydrogen transport to the crack tip is supposed to control the plateau crack velocity.

5.2 Experimental observations

SCC kinetics of high-strength steels are different in water and in gaseous hydrogen as shown by the results from Nelson and Williams (1977). Using double torsion specimens, they conducted experiments at various temperatures and using steels of different yield strengths. Figure 9 shows their data in water at different temperatures for 4130 of yield strength 1330 MPa. Their measurements indicated that the threshold stress intensity factor remained the same, independent of temperature. However, the plateau crack velocity increased by approximately four orders of magnitude when the temperature rose from 1°C to 89°C. In contrast, the corresponding results in gaseous hydrogen (Figure 10) indicated that the threshold stress intensity K_{IH} increased with increasing temperature. However, the plateau crack velocity increased with increasing temperature up to 53°C and then decreased with further increase

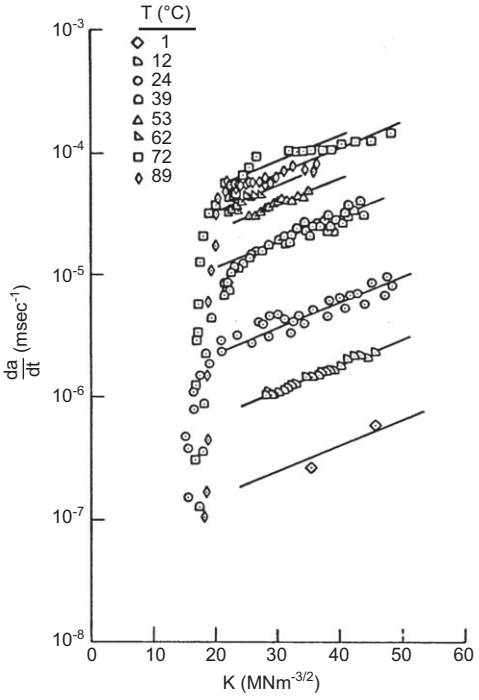

Figure 9 Crack velocity vs. stress intensity factor for 4130 (1330 MPa) in distilled water at various temperatures. Reprinted from Nelson and Williams (1977) with permission from NACE.

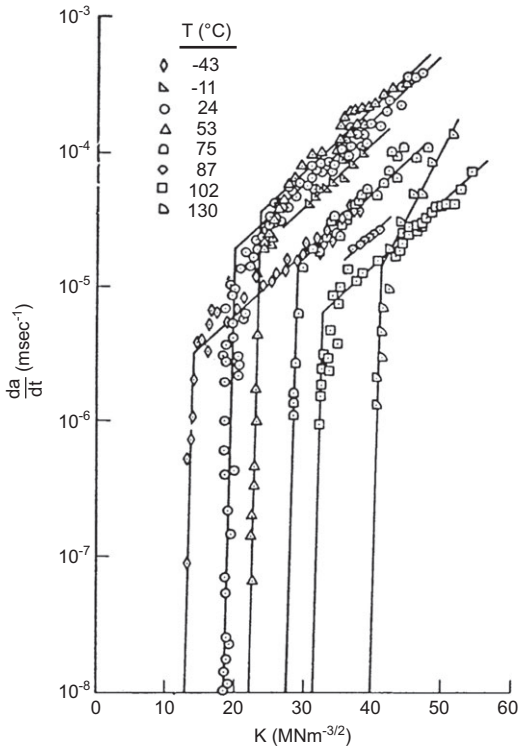

Figure 10 Crack velocity vs. stress intensity factor for 4130 (1330 MPa) in 77.3 kPa gaseous hydrogen at various temperatures. Reprinted from Nelson and Williams (1977) with permission from NACE.

in temperature. In addition, the extent of increase in the plateau crack velocity was not to the same extent as that in water experiments, suggesting that the activation energies for the rate-limiting step were lower than those in water experiments. These results indicated that the crack growth kinetics were different in water and in gaseous hydrogen for the same steel.

Complementary data for the 4340 steel (σ_y=1344 MPa) were generated by Simmons et al. (1978), and their results are presented in Figure 11 (in water) and 2.1 bar (133 kPa gaseous hydrogen). These are the Arrhenius plots of the plateau crack velocity as a function of temperature. For the water experiments (Figure 11), the crack velocity increased with increasing temperature, similar to the results from Nelson and Williams (1977). In contrast, there was a maximum in the crack velocity in gaseous hydrogen (Figure 12). The maximum temperature appears to be slightly greater than that observed by Nelson and Williams. Finally, the activation energy was greater for the water experiments, again similar to the results from the previous study.

Experiments in water at different temperatures have also been conducted by Magdowski (1987a,b), Speidel and Bertilsson (1984), and Speidel and Magdowski (1986) using different low-alloy steels. Their results again

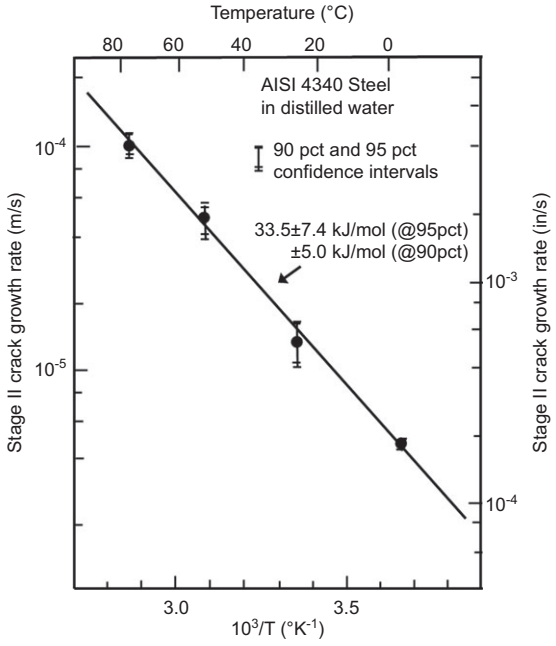

Figure 11 An Arrhenius plot of the plateau crack velocity as a function of temperature for 4340 in water at various temperatures. Reprinted from Simmons et al. (1978) with permission from Springer.

indicated that increases in temperature resulted in the increase in plateau crack velocity, whereas the threshold stress intensity factor remained unaffected. These observations were similar to the results reported by Nelson and Williams (1977) and Simmons et al. (1978).

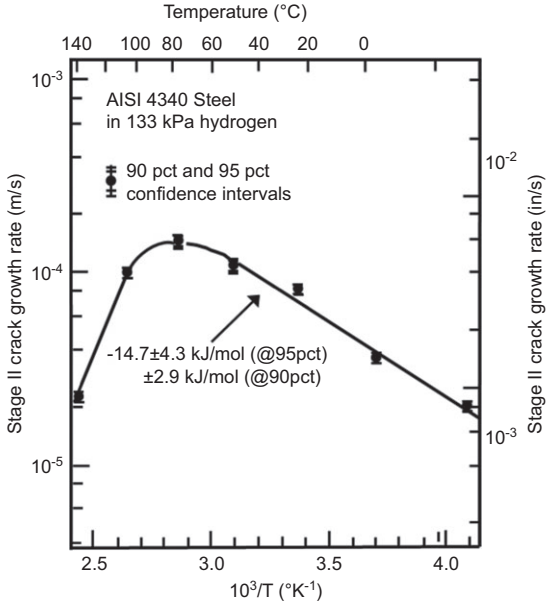

Figure 12 An Arrhenius plot of the plateau crack velocity as a function of temperature for 4340 in 133 kPa hydrogen at various temperatures. Reprinted from Simmons et al. (1978) with permission from Springer.

The effect of yield strength on the crack velocity was also investigated by Magdowski (1987a,b), Speidel and Bertilsson (1984), and Speidel and Magdowski (1986) using a number of low-alloy steels that had been quenched and tempered. Their results, shown in Figures 13 and 14, indicated that the steel composition did not influence the plateau stress corrosion crack velocity and that the plateau crack velocity was controlled by the yield strength. Note that Figure 14 is similar to Figure 1 and also shows the influence of temperature.

The effect of temperature was further investigated by Magdowski (1987a,b), and the results are shown in Figure 15. SCC occurred in two different temperature regimes, each with a specific activation energy. This suggested that the rate-limiting processes and the mechanism of cracking could be different in the two temperature regimes. Galvale (1990) has compared the data from Magdowski with the surface-mobility stress-corrosion-cracking mechanism predictions and observed a good correlation between the predicted and the measured values.

Figure 16 shows the influence of yield strength on the kinetics of SCC in the low-temperature regime (at 23°C). Here, v_{II} increased with the strength of the metal, as is usual for the higher temperatures. K_{ISCC}, instead of being independent of strength, decreased from 49 MPa $m^{1/2}$ at 1025 MPa to 17 MPa $m^{1/2}$ at 1490 MPa. This behavior was similar to that observed by workers such as Chu, Liu, Hsiao, and Li (1981), who worked with high-strength steels at room temperature, but contrary to behavior in the high-temperature regime. Such behavior is similar to the observed behavior in gaseous hydrogen, tending to suggest an HE mechanism of SCC in the low-temperature regime.

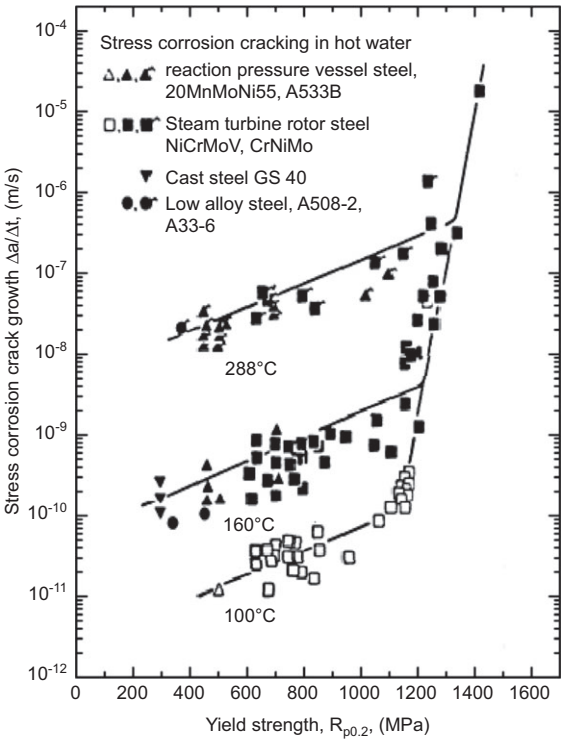

Figure 14 The effect of yield strength and temperature on the crack velocity for low-alloy steels in water. Reprinted from Magdowski (1987) with permission from the Swiss Academy of Science.

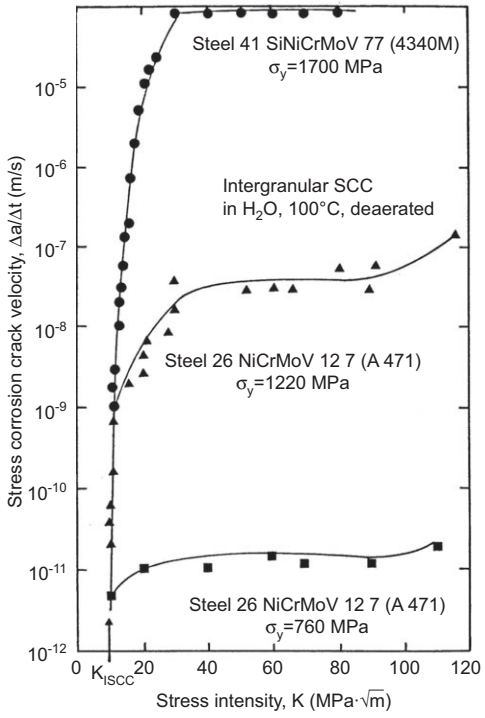

Figure 13 The effect of yield strength on the stress corrosion crack velocity for two different steels in water at 100°C. Reprinted from Speidel (1984) and Speidel and Bertilsson (1984) with permission from Springer.

Rieck (1985) tested two quenched and tempered low-alloy steels in water at 90°C. This is in the high-temperature region of cracking as defined by Figure 15. For conventional heat treatment schedules, producing a range of strengths from 560 to 1700 MPa, the plateau crack velocity, v_{II}, displayed the well-established correlation with strength initially noted by Speidel and Bertilsson (1984), and the results were within the error band of Figure 1. For these conventional heat treatments, austenitizing temperature and prior austenite grain size had no effect on v_{II}. An intercritical heat treatment, however, produced the same crack velocity as the fully austenitized and quenched steel, despite the lower strength and hardness. On the basis of fractography, this behavior was explained in terms of a slight change in the cracking mechanism, with ferrite breaking in a ductile manner, whereas the martensite suffered IGSCC.

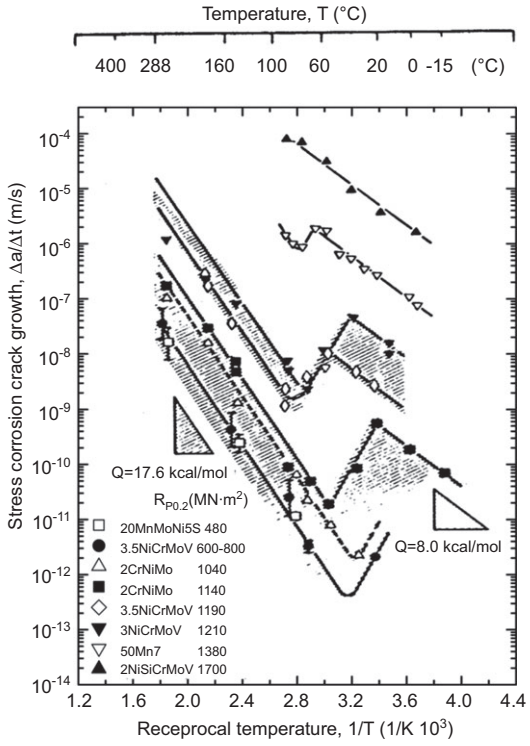

Figure 15 An Arrhenius plot of the crack velocity vs. temperature for a number of steels of different yield strengths. The trends in the plot indicate that there are two distinct temperature regimes for the SCC of these steels. Reprinted from Magdowski (1987) with permission from the Swiss Academy of Science.

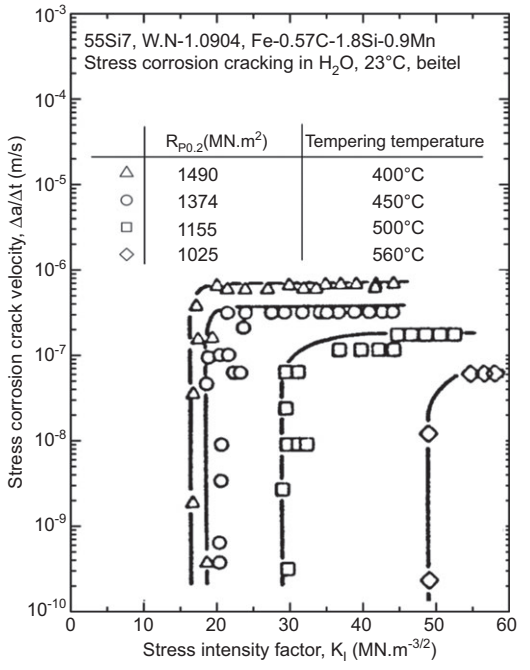

Figure 16 Results in low-temperature water indicating the effect of yield strength on stress corrosion crack velocity and threshold stress intensity factor. Reprinted from Magdowski (1987) with permission from the Swiss Academy of Science.

5.3 Discussion on kinetics of crack growth

The results shown in Figure 15 (Magdowski, 1987a; Speidel & Bertilsson, 1984) indicate two different SCC regimes over the temperatures tested, and with distinct activation energy in each temperature regime. The experiments in low-temperature water (Figure 16) indicate that K_{ISCC} decreased and v_{II} increased with increasing yield strength. These results were similar to the data from Nelson and Williams (1977) for the tests in 77.3 kPa gaseous hydrogen. Moreover, Nelson and Williams also observed a similar trend for cracking experiments in water at 24°C. These results tend to suggest that perhaps the SCC of high-strength steels at room temperature could be controlled by the HE mechanism.

In contrast, the experiments in high-temperature water indicated that K_{ISCC} was not influenced by the yield strength of the material and that the plateau crack velocity, v_{II}, increased with increasing yield strength (Figures 1 and 13). Moreover, the activation energies were also different at the two temperature regimes. These observations suggest that perhaps HE may not be the mechanism of cracking in high-temperature water. AD could be possible and the effect of yield strength on the K_{ISCC} can be explained by the critical strain rate required to continually fracture the passive film at the crack tip (Scully, 1972a,b, 1975, 1980). This also means that the crack tip strain rate is the same for all high-strength steels at a particular temperature irrespective of the yield strength of the steel. This will be one of the topics investigated experimentally in the present study.

6 Hydrogen influence

6.1 Hydrogen mechanisms

Lynch (2003, 2012a,b) reviewed the hydrogen-assisted cracking (HAC) mechanisms. There are three hydrogen-related mechanisms, namely, HEDE, HELP, and adsorption-induced dislocation emission (AIDE). These mechanisms can be applicable to both hydrogen environment embrittlement (HEE) and internal HE (IHE). Although the mechanisms could be common, the rate-limiting step could be different for IHE and HEE – for IHE, hydrogen diffusion may control kinetics, whereas for HEE, hydrogen adsorption process may control the rate of HEE under certain conditions.

Hydrogen-enhanced decohesion proposes the weakening of the metal-metal bonds at or near the crack tip by

the presence of localized hydrogen so that tensile decohesion (separation) of the atoms occurs in preference to slip (Gerberich, Livne, & Chen, 1986; Gerberich, Marsh, & Hoehn, 1996; Oriani, 1972, 1987). Hydrogen at the crack tip or at interstitial sites is thought to result in the decrease of electron-charge density between the metal-metal atoms. Dislocation activity at these locations may also aid decohesion in some instances. Such decohesion and high concentrations of hydrogen are possible at the crack tip, at a region ahead of the crack tip (within the plastic zone), and at the positions of maximum in hydrostatic stress (Gerberich et al., 1996). Crack growth in this case would be expected to occur along GBs; cleavage planes and the fracture surfaces would mostly be featureless except for particles, steps, and tear ridges between the decohered regions.

HELP, according to Lynch (2003), is based on the softening due to the hydrogen atmosphere around mobile dislocations, and obstacles to dislocations, in a volume of material ahead of the cracks (Birnbaum, 1994; Birnbaum & Sofronis, 1994; Birnbaum, Robertson, Sofronis, & Teter, 1997; Oriani, 1972). Because hydrogen diffusion can be rapid in regimes where HAC occurs, these hydrogen atmospheres can rearrange themselves rapidly, thereby minimizing the total elastic energy, and this results in decreased resistance to dislocation motion and to increased dislocation velocities. Because hydrogen tends to localize near crack tips due to hydrostatic stresses or entry of hydrogen into crack tips, deformation locally occurs in these regions. Deformation due to microvoid coalescence is the most likely deformation process, which result in a dimple fracture surface.

AIDE combines the features of both HEDE and HELP mechanisms – weakening of atomic bonds by the presence of hydrogen and crack growth occurring due to localized slip (Lynch, 1977, 1988, 1997). Lynch proposed that the hydrogen on the surface and at the first few atomic layers at the crack tip (adsorbed hydrogen) weakens the interatomic bonds, thereby releasing dislocations from crack tips. Higher stresses are needed for this to occur and combined with the dislocation activity in the plastic zone ahead of the crack tip, small voids at particles or at slip-band intersections occur. Crack growth primarily occurs through alternative slip from crack tips and the formation of microvoids ahead of the crack tip. Void formation also assists in resharpening of the crack so that high aspect ratio is maintained. Fracture surfaces are covered in small shallow dimples, and fracture occurs mostly macroscopically along low-index crystallographic planes.

6.2 HAC processes

HAC can occur through IHE or HEE. For IHE, there has to be a source of hydrogen, and one possibility is the manufacturing processes, such as casting, welding, surface chemical cleaning, and electrochemical machining (Gangloff, 2003). Subcritical crack growth occurs when the hydrogen-charged component is stressed, and this results in a redistribution of hydrogen from the general microstructure to the crack tip process zone. For IHE, stress during hydrogen charging is not needed, and hydrogen production during straining is also not required.

HEE requires both mechanical loading and chemical reaction causing hydrogen production. Atomic hydrogen is produced on clean crack surfaces located close to the crack tip. This is followed by the hydrogen uptake near the fracture process zone, ahead of the crack tip, and subsequent embrittlement process. This case can explain the hydrogen cracking process for the SCC of certain alloy-environment systems. During this process, AD at the crack tip can also occur concurrent with hydrogen production, thus further enhancing the crack growth rate. It is generally accepted that HEE could be responsible for the SCC of high-strength alloy systems.

There are some common features and some differences between IHE and HEE. Both require hydrogen, and damage occurs subcritically at stress intensity factors below K_{IC}. Both follow similar macroscopic crack paths, along intergranular regions, interfacial and/or along certain planes on the grain facets. Both are affected by the applied stress intensity factor, yield strength, loading rate, GB purity, and fracture process zone hydrogen concentration. Both are controlled by strong gradients in hydrogen concentration and stress near the crack tip. A significant difference between the two processes is the kinetics of crack growth. For HEE, kinetics of hydrogen production and mass transport could be the rate-limiting steps. Also, the location of the damage processes ahead of the crack tip differ for both processes (Page & Gerberich, 1982). Factors controlling the damage location, such as the maximum in tensile stress at a region ahead of the crack tip, the plastic strain and the associated dislocation profile about the crack tip, distribution of hydrogen trap sites, and the concentration of environmentally produced hydrogen concentration, could be different for the two HAC processes.

6.3 Hydrogen trapping

One of the significant rate-limiting steps for HAC is hydrogen trapping and transport. It is important to

understand the effect of steel microstructure so that HE can be minimized. All three mechanisms of HAC propose hydrogen diffusion ahead of a stationary or moving crack and affecting the plastic zone ahead of the crack tip. For high-strength steels, likely sites of trapping include carbides, prior austenite GBs, martensitic lath structures, and dislocations (Birnbaum, 1994; Birnbaum & Sofronis, 1994; Escobar, Depover, Duprez, Verbeken, & Verhaege, 2012; Pérez Escobar, Duprez, Atrens, & Verbeken, under review; Pérez Escobar, Duprez, Verhaege, Atrens, & Verbeken, under review; Pérez Escobar, Minambres, Duprez, Verbeken, & Verhaege, 2011; Pérez Escobar, Wallaert, Duprez, Atrens, & Verbeken, under review; Yoo, Lee, Chan, & Morris, 1993). Hydrogen trapping also controls hydrogen solubility and the efficiency of diffusion. Increasing the density of trap sites and the binding energy of hydrogen to a trap decreases hydrogen diffusivity. This minimizes the occurrence of HAC (Pressouyre & Bernstein, 1978; Scully, Van Den Avyle, Cieslak, Romig, & Hills, 1991; Stevens & Bernstein, 1985). Conversely, reversible trap sites provide more hydrogen to areas of triaxial stress state ahead of the crack tip, thereby increasing the likelihood of HAC. Data from the literature suggest that decreasing trap binding energy and increasing hydrogen diffusivity has decreased the threshold stress intensity for 4340 and Aermet 100 (Gangloff, 1984; Nagumo, Nakamura, & Takai, 2001; Thomas, Scully, & Gangloff, 2003; Yamakawa, Yonezawa, & Yoshizawa, 1984).

6.4 Hydrogen transport

Transportation of hydrogen to the degradation site is an important step in HE. Diffusion of hydrogen, the incubation period, and the hydrogen concentration buildup are the important features that reflect the transportation kinetics (Birnbaum, 1994; Birnbaum & Sofronis, 1994). Introduction of the hydrogen atom (from solution in the case of SCC in water) into the lattice results in localized volume (Peisl, 1978) and modulus changes (Mazzolai & Birnbaum, 1985; Mazzolai & Lewis, 1985). As a result, there is diffusion through NILSs toward these regions to eliminate the chemical potential gradient. Hydrogen transported through NILS diffusion can accumulate at various microstructural heterogeneities, such as dislocations, GBs, inclusions, voids, and impurity atoms (Gibala & DeMiglio, 1981; Wert, 1983). Trapping has been observed to be an important part of HE and its significance lies in the embrittling mechanism (Gibala & DeMiglio, 1981; Stevens & Bernstein, 1985).

Hydrogen transport by dislocations toward the crack tip may also be important (Tien et al., 1981). However, more dislocations also move away from the crack tip, thus cancelling the effect of hydrogen transport through dislocations. Moreover, other experimental evidence does not support hydrogen transport by dislocations (Frankel & Latanision, 1986; Ladna & Birnbaum, 1987).

7 Grain boundaries

7.1 Introduction

Grain boundaries (GBs) are regions of mismatch between the adjacent grains, and their structure is different from that of their grain interior. They are areas of high energy. As a consequence, many impurities segregate to them, and they are a preferential site for precipitation of carbides. Some of the metallic properties that are affected by the GB structure and composition include high-temperature creep, superplasticity, recrystallization, yielding, and embrittlement of metals under certain conditions. The embrittlement of metals includes phenomena such as SCC, HE, temper embrittlement, and liquid metal embrittlement.

SCC can occur in the presence of a tensile stress and a corrosive medium. Depending on the steel-environment system, the cracks can proceed along the prior austenite GBs (IGSCC) or through the matrix (TGSCC). IGSCC has been observed in high-strength low-alloy steels in various aqueous environments and in hydrogen at low temperatures (Atrens et al., 1993; Briggs, Airey, & Edwards, 1081; Gao, Lu, & Wei, 1984; Magdowski, 1987a; Padmanabhan, & Wood, 1983; Ramamurthy & Atrens, 1993, 2010; Ramamurthy et al., 2011; Simmons et al., 1978; Wert, 1983). One of the mechanisms proposed for the SCC of these steels advocates preferential dissolution along the prior austenite GBs (AD) for crack advancement. This can be achieved if the grain faces are covered with a passive film so that they are inert, and selective dissolution of the segregants or the precipitates occurs at the GBs, which facilitate crack advancement.

This preferential attack on the GBs has been observed by McLean and Northcott (1948) when their steels were subjected to certain heat treatments. This was supported by the systematic study into the preferential dissolution of the carbides, the interface, and the matrix in aqueous solutions by Cron, Payer, and Staehle (1971). Their results show that depending on the potential and pH conditions, preferential dissolution of one or the other phases occurs in their system. Bandyopadhyay and Briant (1982,

1983) and Bandyopadhyay, Briant, and Hall (1985a,b) have shown that the susceptibility of a NiCrMoV steel to SCC in caustic solutions correlates with the depth of the preferential etching of the prior austenite GBs in a picric acid solution containing tridecyl benzene sulfonate as a wetting agent. They also have correlated the localized corrosion attack on the intergranular facets of NiCrMoV steel, cracking in caustic solutions, to the preferential dissolution of carbides at the GBs (Bandyopadhyay et al., 1985a). These results and the study by Lea (1980) suggest that the tendency of these impurities to promote dissolution at the GBs appears to be electrochemical in nature. This leads to the expectation that the electrochemistry of the GBs could be different from the grain interiors and, in particular, that the potential of the GBs is different from that of the grain interiors, so that preferential dissolution can be achieved. Thus the potential measured at the GBs and at the grain interiors may reveal the differences in the GB electrochemistry and explain why the crack propagation is along the prior austenite GBs.

7.2 GB composition

GB chemistry is of interest as composition differences at GBs could lead to differences in electrochemistry. These differences could be due to carbides at GBs or could relate to the segregation of metalloids. The following work on pipeline steels is reviewed because GB segregation was directly addressed in relation to intergranular SCC. Wang et al. (1998) used analytical electron microscopy (AEM) to measure the composition of GBs and interconstituent boundaries (IBs) of X52 pipeline steel using specimens about 40±60 nm in thickness. All elements of interest were examined with the exception of carbon. With this caveat, there was no segregation at proeutectoid ferrite GBs. This indicated that the commonly expected species S and P are not responsible for preferential corrosion of GBs during IGSCC of pipeline steels. Manganese was the only species measured to segregate at the IBs. Manganese segregated to the IBs between proeutectoid ferrite and pearlitic cementite, and desegregated from IBs between proeutectoid ferrite and pearlitic ferrite. The pearlitic cementite was Mn rich. There was no Mn segregation at the IBs between pearlitic ferrite and pearlitic cementite. The pattern of Mn segregation could be explained in terms of diffusion in the process zone ahead of the pearlite during the austenite to pearlite transformation and diffusion in the IBs between the proeutectoid ferrite and pearlite.

Wang and Atrens (203a) characterized GBs, particularly ferrite: ferrite GBs, of X70 pipeline steel, using AEM in order to understand its IGSCC mechanism(s). The microstructure consisted of ferrite (α), carbides at ferrite GBs, some pearlite, and some small precipitates inside the ferrite grains. The precipitates containing Ti, Nb, V, and N were identified as complex carbonitrides and designated as (Ti, Nb, V)(C, N). The GB carbides occurred (1) as carbides along ferrite GBs, (2) at triple points, and (3) at triple points and extending along the three ferrite GBs. The GB carbides were Mn rich, were sometimes also Si rich, contained no microalloying elements (Ti, Nb, V), and also contained no N. It was not possible to measure the GB carbon concentration due to surface hydrocarbon contamination despite plasma cleaning and glove bag transfer from the plasma cleaner to the electron microscope. Furthermore, there may not be enough X-ray signal from the small amount of carbon at the GBs to enable measurement using AEM. However, the microstructure does indicate that carbon does segregate to α:α GBs during microstructure development. This is particularly significant in relation to the strong evidence in the literature linking the segregation of carbon at GBs to IGSCC. It was possible to measure all other elements of interest. There was no segregation at α:α GBs, in particular no S, P, and N and no segregation of the microalloying elements Ti, Nb, and V.

Atrens, Wang, Stiller, and Andren (2006) carried out critical measurement to understand the IGSCC of pipeline steels: the atom probe field ion microscope (APFIM) measurement of the carbon concentration at a GB. The APFIM measurement was related to the microstructure and to IGSCC observations. The APFIM indicated that the GB carbon concentration of X70 was ~10 at% or less, which correlated with a high resistance to IGSCC for X70. The role of segregation at GBs may be to change GB mechanical properties. This idea is supported by recent work (Wang & Atrens, 2003b) showing that the stress corrosion crack path can be changed from intergranular to transgranular for a commercial pipeline steel.

7.3 GB electrochemistry

GB potential measurements have mainly been carried out for aluminum alloys, and the potential differences between the GBs and the matrix have been correlated to the SCC behavior. One such measurement, for a coarse-grained Al-4% Cu alloy sheet aged to a condition susceptible to intergranular corrosion, was reported by Dix (1940). In one specimen, the GBs were carefully masked off with Bakelite varnish so that only the grain interiors were exposed, and in the other specimen only the GBs were exposed. However, the painting was such that, besides

GBs, the regions adjacent to the GBs were also exposed in the second specimen. The specimen with the exposed GBs was found to be 44 mV more negative than the specimen with the masked GBs when immersed in a sodium chloride/hydrogen peroxide solution. If electrically connected, the GBs would have preferentially corroded. This potential difference would have been higher had it been possible to mask off the GBs accurately.

As a further development of this technique (Dix, 1940), the potential of small local areas on the surface of the same aluminum alloy was measured using a 1-mm capillary tube filled with KCl and connected to a calomel reference electrode. The drop of solution at the end of the capillary (about 1 mm in diameter) was brought in contact with the specimen. It was observed that the measured potential at the GBs is more negative than that at their grain interiors, confirming previous results; and the potential difference was as much as 200 mV in one case.

McLean and Northcott (1948) measured the free corrosion potentials of the fractured steel specimens, subjected to various heat treatments, in 0.1 N $FeCl_2$ solution. As the fracture was intergranular, the potentials were thought to be related to that at the GBs. It was found that the measured potentials were dependent on the tempering temperature and the potential was more positive at 500°C temper, when the impact strength reduced to practically zero.

Doig and Edington (1974) measured the GB potential of aged Al-7.2 wt% Mg and Al-4.4 wt% Cu alloys with respect to the bulk corrosion potential by using microelectrodes in aerated 1 M NaCl. In Al-Mg alloys, precipitation hardening produces Al_3Mg_2 at the GBs, which are anodic compared to the bulk and expected to dissolve preferentially. In Al-Cu alloys, the solution (Cu)-depleted zone adjacent to the GB microelectrodes indeed confirmed the anodic regions in these alloys. But Marek and Starke (1976), using a technique similar to that of Doig and Edington, failed to reproduce these results and concluded that potential differences between the grain and GBs were insignificant in these alloys.

Issacs and Vyas (1981), using a microtip scanning reference electrode, were successfully able to correlate the measured GB potential on a large-grain sensitized type 304 stainless steel to its intergranular corrosion behavior in 2.5 N sulfuric acid. They also showed that the current peak height from one of the GBs closely matched with the polarization curve for this steel.

7.4 Discussion

The previous section indicated that the GBs could be active regions during SCC. Previous investigations indicated that the GBs tend to be more anodic compared to the grain interior, thus providing a favorable path for crack propagation. Such observations could be important if the mechanism of corrosion is shown to be AD in the current system of interest.

8 Influence of applied stress rate

8.1 SCC in water at 90°C

Ramamurthy and Atrens (1993) used the LIST to study the SCC of as-quenched 4340 and 3.5NiCrMoV steel in aerated distilled water at 90°C. The microstructure of the as-quenched 3.5NiCrMoV steel was characterized by Gates, Atrens, and Smith (1987). Figure 17 shows that the as-quenched microstructure was lath martensite, with the prior austenite GBs clearly visible. Microtwins were present within the laths. There was retained austenite, with the retained austenite more prevalent at lath boundaries.

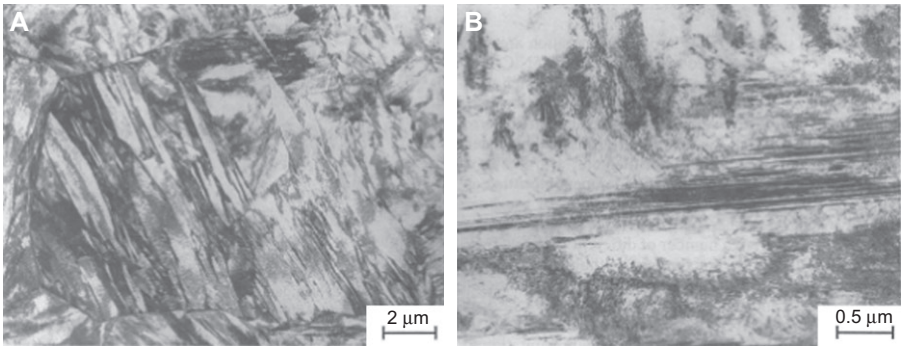

Figure 17 Microstructure of the as-quenched 3.5NiCrMoV steel. Reprinted from Gates et al. (1987) with permission from Wiley. (A) Lath martensite microstructure structure and prior austenite GBs and (B) microtwins within a martensitic lath in the as-quenched steel.

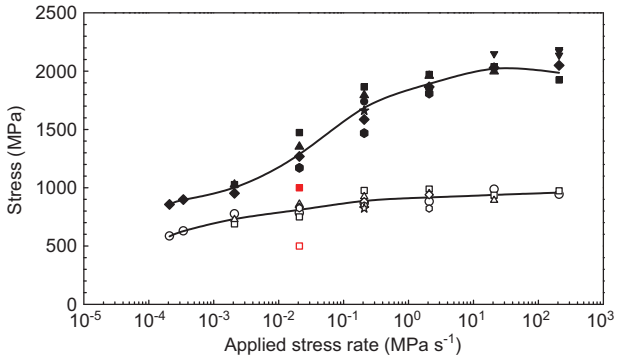

Figure 18 Results from LIST tests plotted as a function of applied stress rate for as-quenched 4340 in aerated distilled water at 90°C (Ramamurthy & Atrens, 1993). The open symbols represent the threshold stress for SCC and the closed symbols represent the fracture stress. Similar open and closed symbols represent data from the same specimen. The triangles at the two highest applied stress rates represent the tests where there was no stress corrosion. Open and closed red squares represent the threshold and the fracture stresses for a specimen immersed in water at 90°C for 14 days before the test was carried out at 0.02 MPa s^{-1}.

Figure 18 shows that there was SCC at all applied stress rates in 4340, but not at applied stress rates higher than 0.034 MPa/s for the 3.5NiCrMoV steel. In both steels, the stress corrosion crack velocity was strongly dependent on the applied stress rate (Figure 19). The fracture surface morphology was intergranular in all cases. Corrosion pits influenced stress corrosion crack initiation.

8.2 SCC in distilled water at 30°C

Ramamurthy and Atrens (2010) conducted LISTs in 30°C aerated distilled water using as-quenched 4340 and 3.5NiCrMoV steels. SCC occurred at all applied stress rates for 4340 steel (Figure 20), whereas only at applied stress rates ≤0.002 MPa s^{-1} for the 3.5NiCrMoV steel (Figure 21). The crack velocity increased with increasing applied stress rate for both steels with the maximum crack velocity for 4340 steel corresponding to v_{II} in fracture mechanics tests in room temperature water. The crack velocity was similar to that in 90°C water (Figure 22).

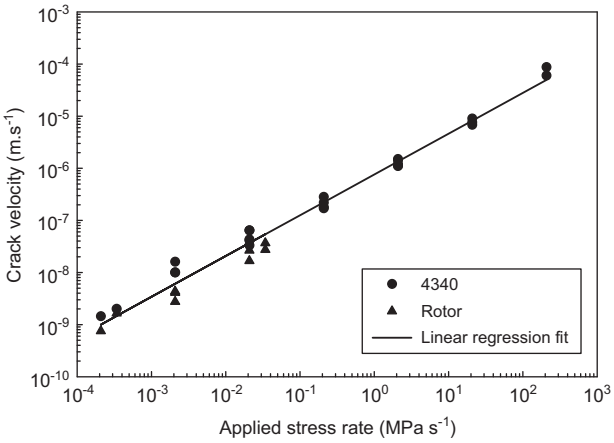

Figure 19 Average crack velocity plotted as a function of the applied stress rate for as-quenched 4340 and 3.5NiCrMoV rotor steel in aerated distilled water at 90°C (Ramamurthy & Atrens, 1993).

8.3 SCC under conditions of cathodic hydrogen charging

Ramamurthy et al. (2011) studied SCC of as-quenched 4340 and 3.5NiCrMoV steels under hydrogen-charging conditions, with a cathodic current applied to the gauge length of specimens using LISTs in 0.5 M H_2SO_4 solution containing 2 g/l arsenic trioxide (As_2O_3) at 30°C. Both the fracture and the threshold stress decreased with decreasing applied stress rate (Figure 23) and were substantially lower than corresponding values measured in distilled water at 30°C at the open circuit potential. The threshold stress values correspond to 0.03–0.08 σ_y for 4340 and 0.03–0.2 σ_y for the 3.5NiCrMoV steel. SCC velocities, at the same applied stress rate, were an order of magnitude greater than those in distilled water (Figure 24). However, the plots of the crack velocity vs. applied stress rate had similar slopes, suggesting the same rate-limiting step. The fracture surface morphology was mostly intergranular, with quasi-cleavage features.

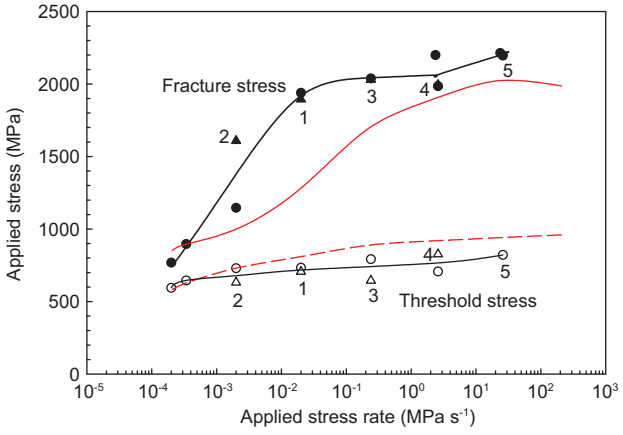

Figure 20 A plot of fracture stress (closed symbols) and threshold stress (open symbols) plotted as a function of the applied stress rate for as-quenched 4340 in distilled water at 30°C (Ramamurthy & Atrens, 2010). The numbers 1 to 5 correspond to the potential drop data. The data from 90°C water tests are shown as red lines (Ramamurthy & Atrens, 1993).

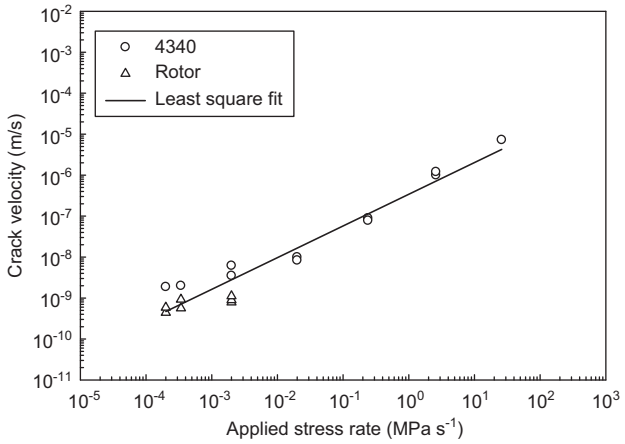

Figure 21 Average crack velocity plotted as a function of applied stress rate for both steels (Ramamurthy & Atrens, 2010).

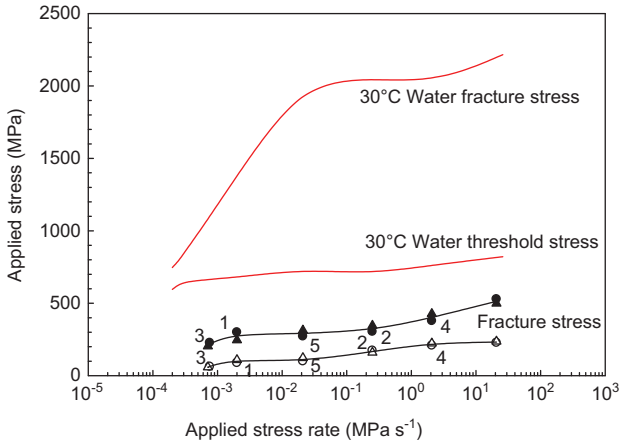

Figure 23 A plot of fracture stress (closed symbols) and threshold stress (open symbols) plotted as a function of the applied stress rate for as-quenched 4340 under hydrogen-charging condition at 30°C (Ramamurthy et al., 2011). The numbers 1 to 5 correspond to the potential drop data not presented here. The red trend lines represent the polynomial regression data from the 30°C water experiments (Ramamurthy & Atrens, 2010).

8.4 Fracture stress and threshold stress

Figure 18 indicated that for the 90°C water experiments (Ramamurthy & Atrens, 1993), the fracture and the threshold stresses remained constant at higher applied stress rates and decreased with the applied stress rate at applied stress rates <0.2 MPa s^{-1}. For 4340, the fracture stresses at low applied stress rates were ~0.4 σ_{fo}, where σ_{fo} was the fracture stress in air. The threshold stresses were much lower, ~0.25 σ_{fo} at low applied stress rates. For the 3.5NiCrMoV steel, the corresponding values were ~0.6 and 0.4 σ_{fo} for the fracture and threshold stresses, respectively. These values were comparable to the 30°C water data (Figure 20; Ramamurthy & Atrens, 2010), ~0.4 and 0.3 σ_{fo} for the fracture and threshold stresses of 4340 steel, and 0.6 and 0.35 σ_{fo} for the fracture and threshold stresses of 3.5 NiCrMoV steel, respectively. These values also correspond to 0.35 and 0.47 σ_y for 4340 and 3.5 NiCrMoV steel, where σ_y is the yield stress. Thus 4340 can be considered to be more susceptible to SCC because the onset of SCC occurred at a much lower fraction of σ_y, and the specimen failed at much lower σ_{fo}.

Comparison with data from the literature indicates that the initiation stress was found just above

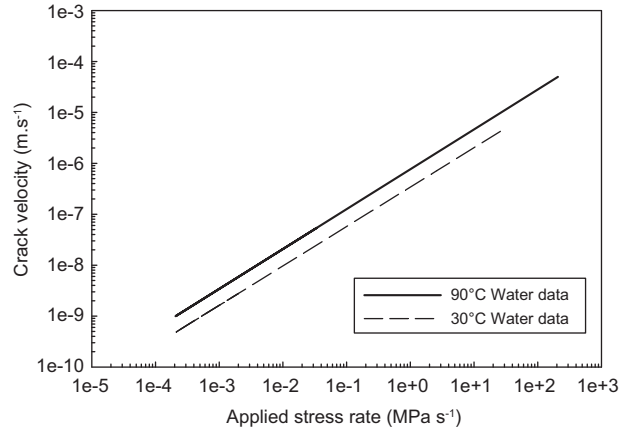

Figure 22 Linear square fit plots of average stress corrosion crack velocity as a function of applied stress rate for 30°C water (dash line) and 90°C water (solid line) for both steels (Ramamurthy & Atrens, 2010).

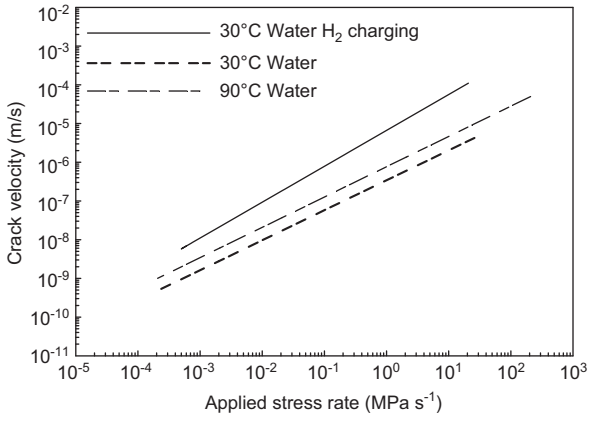

Figure 24 Linear square fit plots of average stress corrosion crack velocity as a function of applied stress rate under hydrogen-charging condition at 30°C (solid line) (Ramamurthy et al., 2011), at open circuit potential in 30°C water (medium dash line) (Ramamurthy & Atrens, 2010) and at open circuit potential in 90°C water (dark dash line) (Ramamurthy & Atrens, 1993) for both steels.

the yield stress for a range of pipeline steels undergoing SCC in high-pH carbonate-bicarbonate solution (Wang & Atrens, 1996). Furthermore, rock bolt SCC was found to have a threshold stress close to the ultimate tensile strength (Gamboa & Atrens, 2003a, 2005; Villalba & Atrens, 2008a). Moreover, SCC in Mg-Al alloys was also associated with hydrogen; the threshold stress was found to be about 0.5 σ_y also in the elastic region of applied stress (Winzer, Atrens, Dietzel, Raja, et al., 2008; Winzer, Atrens, Dietzel, Song, et al., 2008; Winzer et al., 2007). These observations indicate that the threshold stress depends on the particular metal-environment couple.

In the 90°C water experiments, at low applied stress rates, stress corrosion cracks initiated from corrosion pits, which agreed with the data from other low-alloy steels (Magdowski, 1987b; Parker, 1973). Corrosion pits provide a local stress concentration and locally favorable electrochemical conditions, so that stress corrosion cracks could be initiated at values of the applied stress lower than in those specimens where stress corrosion cracks did not initiate from corrosion pits. Figure 18 indicated that at low applied stress rates, the threshold stress can be decreased by allowing time to develop deeper corrosion pits; the decrease in the fracture stress was mainly due to the early crack initiation, as the crack velocity was the same as in other tests carried out at the same applied stress rate. Moreover, the threshold stresses measured for the specimens left in water at 90°C for 14 days and tested after that period at 0.02 MPa s^{-1} were lower than those for specimens tested at the two slowest applied stress rates; at these slowest stress rates, the specimens were immersed in 90°C water for much more than 14 days before crack initiation was observed. This indicates that there is a synergism between strain rate and the presence of preexisting pits.

In contrast to the water experiments, the fracture stress values measured under hydrogen-charging conditions (Figure 23; Ramamurthy et al., 2011) were ~0.09 to 0.23 σ_{fo} for 4340 and 0.11 to 0.25 σ_{fo} for the 3.5NiCrMoV steel. These values are much lower than in water experiments (Ramamurthy & Atrens, 2010), in which the fracture stress for the 4340 steel ranged from 0.3 to 0.95 σ_{fo} and 0.571 to 0.98 σ_{fo} for the 3.5NiCrMoV steel. Thus, these results indicate that the hydrogen charging significantly decreased the fracture stress for both steels. Also, these values were lower than the extent of the decrease in fracture stress for the slow strain rate testing of hydrogen-charged 4135 steel specimens (tensile strength, 1450 MPa) (Wang, Akiyama, & Tsuzaki, 2007). In that study, the fracture stress decreased to ~0.3 σ_{fo} for the specimens containing 1.3 ppm diffusible hydrogen. One difference between that study and that of Ramamurthy and Atrens was the dynamic charging employed by Ramamurthy and Atrens, which means that the hydrogen fugacity would be much greater, consistent with the larger decrease in the fracture stress.

Lijie, Wuyang, Huijun, Jimei, and Peixin (1993) studied the hydrogen-facilitated SCC of 310 stainless steel and observed that hydrogen reduced the stability of the passive film and shortened the incubation of SCC, resulting in the decrease of threshold stress. However, the mechanism of cracking could be different in stainless steel compared to the high-strength steels examined by Ramamurthy et al. (2011). Under hydrogen charging, the threshold stress also decreased with decreasing applied stress rate. This is in contrast to the water data (Ramamurthy & Atrens, 1993, 2010), where for 4340 the threshold stress remained constant at higher applied stress rates and decreased with the applied stress rate at lower applied stress rates. The different behavior under hydrogen charging could be attributed to the longer test duration at lower applied stress rates, which resulted in greater hydrogen concentrations within the steel due to the dynamic charging employed (Ramamurthy et al., 2011). In fact, a plot of threshold stress vs. logarithm of the test duration or the total accumulated charge would yield a linear fit with the threshold stress decreasing proportionately with the accumulated hydrogen in the steel. Such behavior was also observed previously; Zhang et al. (2007) observed such a linear relationship when hydrogen-assisted cracking experiments were performed in high-strength T-250 maraging steel.

In summary, the threshold stress was controlled by the events occurring at the specimen surface, and the fracture stress was controlled by the crack velocity, which is discussed in the next section.

8.5 Crack tip strain rate and crack velocity

In fracture mechanics tests, SCC is not observed for a stress intensity factor below the threshold stress intensity factor K_{ISCC}. As shown by Speidel and Bertilsson (1984), when the stress intensity factor increases above K_{ISCC} toward the plateau stress intensity (K_p), the crack velocity increases rapidly, and this is region I of the crack velocity v vs. K plot. At stress intensity factors above K_p, the crack velocity remains a constant (v_{II}). The results presented by Ramamurthy and Atrens (1993, 2010) and Ramamurthy et al. (2011) indicate that the crack velocity increased with

increasing applied stress rate and the crack tip strain rate for both steels, until it reached the maximum crack velocity. This maximum crack velocity observed in water experiments corresponded to v_{II} in fracture mechanics tests (Magdowski, 1987a,b; Magdowski & Speidel, 1988; Speidel & Bertilsson, 1984; Speidel & Magdowski, 1986) especially for 4340 in water (Magdowski, 1987a,b; Magdowski & Speidel, 1988; Speidel & Bertilsson, 1984). This suggests that the crack velocity-applied stress rate plots presented in Figures 19, 21, 22, and 24 can be considered to represent region I of the fracture mechanics tests. These plots also indicated that no influence of the steel composition on the crack velocity could be identified for the steels under investigation and that the crack velocities depended only on the applied stress rate, i.e., similar crack velocities were observed at the same applied stress rates.

The methodology for determining the crack tip strain rate and the crack tip strain rate-applied stress rate plots indicate that the applied stress rate controlled the crack tip strain rate as well; the crack tip strain rate increased proportionally with increasing applied stress rate. The crack tip strain rate values were not influenced by the steel composition for the steels investigated by Ramamurthy and Atrens (1993, 2010) and Ramamurthy et al. (2011) and dependent only on the applied stress rate. Using the maximum and minimum crack velocities observed previously (Magdowski, 1987a,b; Magdowski & Speidel, 1988; Speidel & Bertilsson, 1984), it was possible to calculate the critical applied stress rate and the critical crack tip strain rates under the experimental conditions employed.

LIST experiments under various experimental conditions also highlight the importance of the crack tip strain rate in the SCC of these high-strength steels. The crack velocity (v)-crack tip strain rate ($\dot{\varepsilon}_c$) was modeled using the equation $v=A\dot{\varepsilon}_c^m$, where A and m are constants. The values of the exponents ranged from 0.73 to 0.93 for both 4340 and 3.5NiCrMoV steels in 90°C and 30°C water experiments. Even the experiments under hydrogen-charging conditions, presented in Figure 24, exhibited similar exponents for the crack velocity-crack tip strain rate plots. Moreover, typical slopes for log v vs. log $\dot{\varepsilon}$ plots were of the order of 0.5 to 0.7 for IGSCC and 0.2 to 0.3 for TGSCC (Serebrinsky, Duffo, & Galvele, 1999). Fracture surface morphology indicated that there was more IGSCC than TGSCC, and the exponent values from these measurements ranged from 0.73 to 0.93. Thus, the observations from Ramamurthy and Atrens (1993, 2010) and Ramamurthy et al. (2011) were consistent with the literature data. Also, the exponent values observed by Ramamurthy and Atrens and Ramamurthy et al. were greater than those reported for the SCC of stainless steels (0.3 to 0.5) in high-temperature water (Ford, 1981; Ford & Emigh, 1985; Maiya, 1987; Maiya & Shack, 1983), but were within the range 0.5 to 1.0 reported for sensitized stainless steels in high-temperature water (Lidbury, 1983).

Figures 20, 23, and 24 indicated that the stress corrosion crack velocity was dependent on the crack tip strain rate and increased with increasing crack tip strain rate at applied stress rates where there was SCC. Both the 4340 and the 3.5NiCrMoV steel exhibited similar crack velocities at corresponding crack tip strain rates. These observations indicated that the crack velocity was dependent only on the applied stress/strain rate and was independent of the composition of the steels. This result is analogous to that observed in region I of the fracture mechanics tests for these steels in high-temperature water (Speidel & Bertilsson, 1984), where the experimental data for these steels lie on the same vertical band. Such observation was also substantiated by the extensive study conducted by the same group (Magdowski, 1987a,b; Magdowski & Speidel, 1988; Speidel & Magdowski, 1986). These observations imply a similar rate-limiting step, independent of steel composition, for the two steels employed by Ramamurthy and Atrens (1993, 2010) and Ramamurthy et al. (2011).

Sections 3–7 discussed the possible rate-limiting steps that could occur during the SCC of high-strength steels. For the AD mechanism, the role of crack tip strain rate is to rupture the surface film to facilitate dissolution at the crack tip (Ford & Andresen, 2002; Lu & Shoji, 2006; Newman, 1981; Scully, 1980; Vermilyea, 1977). For any mechanisms involving hydrogen, the role of crack tip strain rate is to rupture a surface film that hinders hydrogen ingress into the material. The crack tip strain rate could control the rupture rate of the passive/surface film, thus promoting dissolution and/or hydrogen production and transport. For the experiments under hydrogen-charging conditions, the crack tip strain rate could control the processes affecting the hydrogen transport to the crack tip, such as the dislocation motion and pile up at the crack tip. In addition, the crack tip strain rate could also control the film rupture events, thus creating a bare metal region, which would also facilitate some corrosion at the crack tip and would facilitate hydrogen entry. Thus, the role of the applied stress rate was to produce a crack tip strain rate above the critical crack tip strain rate required for film rupture. The increase in the crack tip strain rate through the increase in the applied stress rate could increase the film rupture rate and/or the production and the transport of hydrogen to the regions ahead of the crack tip.

The increase in the crack tip strain rate through the increase in the applied stress rate could increase the film rupture rate and hence accelerate subsequent events. This acceleration would continue until the maximum crack velocity corresponding to the plateau crack velocity, v_{II}, observed in fracture mechanics tests at corresponding temperatures, is reached, at which point the crack tip remains film free and other processes like transportation of the ionic species to and from the crack tip take over as the rate-limiting step.

Although it appears that there is good evidence for the rate-limiting step being film rupture rate, the actual mechanism of cracking could be different under different experimental conditions. Magdowski (1987a,b) reported that the crack growth rate-temperature plots have different slopes in the high (approx. above 60°C) and low-temperature regions for the experiments in water. The slope in the low-temperature region was consistent with the HE mechanism, and the high-temperature region slope was consistent with the AD mechanism. Their work was supported by the work of Rieck et al. (1988, 1989). Ramamurthy and Atrens (1993, 2010) and Ramamurthy et al. (2011) could not reveal which of these two mechanisms operate in 90°C and 30°C water, respectively. However, the suggestion of HE to be the mechanism of cracking would agree with the results presented by Ramamurthy and Atrens and Ramamurthy et al., as the rate of hydrogen production is dependent on the rate of corrosion at the crack tip, which in turn depends on the rate of film rupture and hence on the crack tip strain rate and the applied stress rate.

For the hydrogen-charging experiments, it is proposed that the increase in the crack tip strain rate through the increase in the applied stress rate could increase the film rupture rate and hence accelerate the hydrogen diffusion and transport processes occurring at regions ahead of the crack tip. Because the hydrogen is generated externally and not produced as a result of film rupture at the crack tip, the role of crack tip strain rate is to aid in the hydrogen transport and diffusion processes only. Thus, it is conceivable that the increase in the crack tip strain rate would increase the hydrogen diffusion/transport rate further, thus resulting in greater crack velocities.

8.6 Fracture morphology and GB properties

LIST experiments in distilled water and under hydrogen-charging conditions indicated that the fracture morphology was mostly intergranular in both steels (Ramamurthy & Atrens, 1993, 2010; Ramamurthy et al., 2011). At some applied stress rates, transgranular regions, ductile fracture, and plasticity were also observed. Mostly intergranular fracture suggests that the fracture path could be along the prior austenite GBs. Evidence for increased dissolution at GBs due to carbide precipitation can be found in the literature (Arioka, Yamada, Terachi, & Chiba, 2006; Arioka, Yamada, Terachi, & Staehle, 2006; Hertzberg & Was, 1998; Rebak, Xia, & Szklarska-Smialowska, 1993).

Another model for the intergranular cracking that fits the experimental data presented in Ramamurthy and Atrens (1993, 2010) and Ramamurthy et al. (2011) is that proposed by Rieck et al. (1989) and Rieck, Atrens, Ramamurthy, Gates, and Smith (1990), which suggested that the crack path is defined by the surface where most dislocations meet. Other than the slip steps, the next obstacle the dislocations meet is the GB. In low-alloy steels, the prior austenite GBs are high-angle GBs and present a more significant obstacle to dislocation motion than the twin boundaries in martensite. This pileup of dislocations at the prior austenite GBs produces concentration ledges and could lead to dissolution of these ledges, causing cracking to be intergranular.

8.7 Discussion

LISTs were performed in distilled water at two different temperatures and under cathodic hydrogen-charging conditions (Ramamurthy & Atrens, 1993, 2010; Ramamurthy et al., 2011). The results indicated that the applied stress rate controlled the crack tip strain rate and the stress corrosion crack velocity. The crack velocity increased with increasing applied stress rate until the maximum crack velocity, corresponding to v_{II} in fracture mechanics tests, was observed in distilled water experiments. Moreover, the crack velocity was dependent only on the crack tip strain rate and the applied stress rate and was not influenced by the composition of the two steels investigated in this study. The results also indicated that the crack tip strain rate controlled the rate-limiting step for the SCC of high-strength steels. The rate-limiting step could be the rupture of a passive/surface film, which would control the rate of metal dissolution and/or the production and transport of hydrogen at the crack tip or at the regions ahead of the crack tip.

Received June 27, 2012; accepted December 13, 2012; previously published online February 25, 2013.

References

Andresen PL, Angeliu TM, Young LM. Immunity, thresholds, and other SCC fiction. In: Chemistry and electrochemistry of stress corrosion cracking: a symposium honoring the contributions of R.W. Staehle. 2001: 65–82.

Andresen PL, Young LM, Catlin GM, Gordon GM. Stress-corrosion-crack initiation and growth-rate studies on titanium grade 7 and alloy 22 in concentrated groundwater. Metall Mater Trans A 2005; 36: 1187–1198.

Arioka K, Yamada T, Terachi T, Chiba G. Influence of carbide precipitation and rolling direction on intergranular stress corrosion cracking of austenitic stainless steels in hydrogenated high-temperature water. Corrosion 2006; 62: 568–575.

Arioka K, Yamada T, Terachi T, Staehle RW. Intergranular stress corrosion cracking behavior of austenitic stainless steels in hydrogenated high-temperature water Corrosion 2006; 62: 74–83.

ASTM. Stress corrosion cracking: The slow strain-rate technique. STP 665. Philadelphia, PA: ASTM, 1979.

Atrens A, Oehlert A. Linearly increasing stress testing of carbon steel in 4 N $NaNO_3$ and in Bayer liquor. J Mater Sci 1998; 33: 783–788.

Atrens A, Wang ZF. ESEM observations of SCC initiation for 4340 high strength steel in distilled water. J Mater Sci 1998; 33: 405–415.

Atrens A, Brosnan CC, Ramamurthy S, Oehlert A, Smith IO. Linearly increasing stress test (LIST) for SCC research. Meas Sci Technol 1993; 4: 1281–1292.

Atrens A, Wang JQ, Stiller K, Andren HO. Atom probe field ion microscope measurements of carbon segregation at an α:α grain boundary and service failures by intergranular stress corrosion cracking. Corros Sci 2006; 48: 79–92.

Atrens A, Winzer N, Song G, Dietzel W, Blawert C. Stress corrosion cracking and hydrogen diffusion in magnesium. Adv Eng Mater 2006; 8: 749–51.

Ayer R, Machmeier PM. Transmission electron microscopy examination of hardening and toughening phenomena in Aermet 100. Metall Trans A 1993; 24: 1943–1955.

Bandyopadhyay N, Briant CL. The Effect of phosphorus on intergranular caustic cracking of NiCr steel. Corrosion 1982; 38: 125.

Bandyopadhyay N, Briant CL. Caustic stress corrosion cracking of NiCrMoV rotor steels – The effects of impurity segregation and variation in alloy composition. Metall Trans A 1983; 14: 2005–2019.

Bandyopadhyay N, Briant CL, Hall EL. Carbide precipitation, grain boundary segregation, and temper embrittlement in NiCrMoV rotor steels. Metall Trans A 1985a; 16: 721–737.

Bandyopadhyay N, Briant CL, Hall EL. The effect of microstructural changes on the caustic stress corrosion cracking resistance of a NiCrMoV rotor steel. Metall Trans A 1985b; 16: 1333–1344.

Bath CF, Troiano AR. Corrosion 1972; 28: 259–263.

Bauernfeind D, Haberl J, Mori G, Falk H. Influence of cold deformation on stress corrosion cracking resistance of highly alloyed austenitic stainless steels in chloride media. In: NACE – International Corrosion Conference Series, Corrosion 2006. Houston, TX: NACE, 2006: 065041–0650417.

Beachem CD. New model for hydrogen-assisted cracking (hydrogen embrittlement). Met Trans 1972; 3: 437–451.

Beghini M, Benamati G, Bertini L. Hydrogen embrittlement characterization by disk pressure tests: test analysis and application to high chromium martensitic steels. J Eng Mater Technol 1996; 118: 179–185.

Bennett DC. Tappi J 1981; 64: 75.

Bianchi GL, Galvele JR. Embrittlement of copper by the surface mobility mechanism. Corros Sci 1987; 27: 631–635.

Bianchi GL, Galvele JR. Stress corrosion cracking of silver alloys in gaseous environments – bromine vapour. Corros Sci 1994; 36: 611–619.

Birnbaum HK. Hydrogen effects on deformation-relation between dislocation behavior and the macroscopic stress-strain behavior. Scr Metall Mater 1994; 31: 149–53.

Birnbaum HK, Sofronis P. Hydrogen-enhanced localized plasticity – A mechanism for hydrogen-related fracture. Mater Sci Eng, A 1994; 176: 191–202.

Birnbaum HK, Robertson IM, Sofronis P, Teter D. In: Magnin T, editor. Second international conference on corrosion-deformation interactions. London, UK: The Institute of Materials, 1997: 172–195.

Briggs A, Airey R, Edwards BC. J Mater Sci 1081; 16: 125.

Brown BF. Stress corrosion cracking of high strength steels. In: Scully JC, editor. Theory of stress corrosion cracking in alloys. NATO, 1971: 186–204.

Buckley P, Placzankis B, Lowder L, Brown IG, Brown R. Noble metal implantation to reduce hydrogen embrittlement in steels. Surf Coat Technol 1991; 49: 500–503.

Chu WW, Liu TH, Hsiao CM, Li SQ. Mechanism of stress corrosion cracking of low alloy steel in water. Corrosion 1981; 37: 320–327.

Coleman EG, Weinstein D, Rostoker W. On surface energy mechanism for stress-corrosion cracking. Acta Metall 1961; 9: 491–496.

Cron CJ, Payer JH, Staehle RW. Corrosion 1971; 27: 1.

Daw MS, Baskes MI. Embedded-atom method: derivation and application to impurities, surfaces, and other defects in metals. Phys Rev B: Condens Matter Mater Phys 1984; 29: 6443–6453.

De Moraes FD, Bastian FL, Ponciano JA. Influence of dynamic straining on hydrogen embrittlement of UNS-G41300 and UNS-S31803 steels in a low H2S concentration environment. Corros Sci 2005; 47: 1325–1335.

Diegle RB, Vermilyea DA. Strain enhanced corrosion in the iron-caustic system. Corrosion 1976; 32: 353–357.

Dietzel W. Stress corrosion cracking in metals. In: Buschow KHJ, Cahn RW, Flemings MC, Ilschner B, Kramer EJ, Mahajan S, editors. Encyclopedia of materials: science and technology. Amsterdam: Elsevier Science Ltd., 2001: 8883.

Dix EH. Acceleration of rate of corrosion by high constant stresses. Trans Am Inst Min Metall Eng 1940; 137: 11–40.

Doig P, Edington JW. Use of microelectrodes in the study of stress corrosion in Aged Al–7·2 wt-% Mg and Al–4·4 wt-% Cu alloys. Br Corros J 1974; 9: 88–90.

Du Z-Y, Tao Y-Y, Li Y-T. Sulfide stress corrosion cracking and weldability of domestic X70 pipeline steel. Trans China Weld Inst 2004; 25: 13–16.

Duffo GS, Galvele JR. S.C.C. of silver alloys due to surface mobility. Corros Sci 1988; 28: 207–210.
Duffo GS, Galvele JR. Experimental confirmation of the surface mobility-stress corrosion cracking mechanism. Ag-15Pd, Ag-15Au and Ag-30Cd alloys in halide and sulphate containing solutions. Corros Sci 1990; 30: 249–265.
Dutton R, Nuttall K, Puls MP, Simpson LA. Mechanisms of hydrogen induced delayed cracking in hydride forming materials. Metall Trans A 1977; 8: 1553–1562.
Eliaz N, Shachar A, Tal B, Eliezer D. Characteristics of hydrogen embrittlement, stress corrosion cracking and tempered martensite embrittlement in high-strength steels. Eng Failure Anal 2002; 9: 167–184.
Escobar DP, Depover T, Duprez L, Verbeken K, Verhaege M. Combined thermal desorption spectroscopy, differential scanning calorimetry, scanning electron microscopy and X-ray diffraction study of hydrogen trapping in cold deformed TRIP steel, Acta Mater 2012; 60: 2593–2605.
Fang BY, Atrens A, Wang JQ, Han EH, Zhu ZY, Ke W. Review of stress corrosion cracking of pipeline steels in “low” and “high” pH solutions. J Mater Sci 2003; 38: 127–132.
Farina SB, Duffo GS. Intergranular to transgranular transition in the stress corrosion cracking of Zircaloy-4. Corros Sci 2004; 46: 2255–2264.
Farina SB, Duffo GS, Galvele JR. Stress corrosion cracking of zirconium and Zircaloy-4 in iodine-alcoholic solutions. Corrosion 2003; 59: 436–442.
Farina SB, Duffó GS, Galvele JR. Stress corrosion cracking of hexagonal close-packed metals and alloys in solutions of iodine in methanol. Corrosion 2005a; 61: 847–856.
Farina SB, Duffo GS, Galvele JR. Stress corrosion cracking of metals and alloys effect of the exchange current density. In: Proceedings of the European Corrosion Congress (EUROCORR 2005). 2005b: 9.
Flanagan TB, Mason NB. The effect of stress on hydride precipitation. Scr Metall 1981; 15: 109–112.
Ford FP. Report No. 81CRD125. New York: General Electric Company, 1981.
Ford FP. Mechanisms of environmental cracking in systems peculiar to the power generation industry. Electric Power Research Report, EPRI NP, September 1982.
Ford FP. Current understanding of the mechanisms of stress corrosion and corrosion fatigue. In: ASTM special technical publication. 1984: 32–51.
Ford FP, Andresen P. In: Marcus P, editor. Corrosion mechanisms in theory and practice. New York: Marcel Dekker, 2002: 605–642.
Ford FP, Emigh PW. The prediction of the maximum corrosion fatigue crack propagation rate in the low alloy steel-de-oxygenated water system at 288°C. Corros Sci 1985; 25: 673–692.
Frandsen JD, Paton NE, Marcus HL. The influence of low-pressure hydrogen gas on crack growth in T.D.-nickel and T.D.-nichrome. Scr Metall 1973; 7: 409–414.
Frankel GS, Latanision RM. Hydrogen transport during deformation in nickel: Part I. Polycrystalline nickel. Metall Trans A 1986; 17: 861–867.
Galvele JR. Enhanced surface mobility as the cause of stress corrosion cracking. J Electrochem Soc 1986; 133: 953–954.
Galvele JR. Surface mobility-stress corrosion cracking mechanism of steels for steam turbine rotors. Corros Sci 1990; 30: 955–958.
Galvele JR. Surface mobility mechanism of stress-corrosion cracking. Corros Sci 1993; 35: 419–434.
Galvele JR. Comments on “Notes on the surface mobility mechanism of stress-corrosion cracking”, by K. Sieradzki and F.J. Friedersdorf. Corros Sci 1994; 36: 901–910.
Galvele JR. Application of the surface-mobility stress corrosion cracking mechanism to nuclear materials. J Nucl Mater 1996; 229: 139–148.
Galvele J. Reply to “Notes on the discussion concerning ‘surface mobility mechanism’ of stress corrosion cracking” by E.M. Gutman. Corros Sci 2003; 45: 2119–2128.
Gamboa E, Atrens A. Environmental influence on the stress corrosion cracking of rock bolts. Eng Failure Anal 2003a; 10: 521–558.
Gamboa E, Atrens A. Stress corrosion cracking fracture mechanisms in rock bolts. J Mater Sci 2003b; 38: 3813–3829.
Gamboa E, Atrens A. Material influence on the stress corrosion cracking of rock bolts. Eng Failure Anal 2005; 12: 201–235.
Gangloff RP, editor. Embrittlement by the localized crack environment. Warrendale, PA: The Minerals, Metals & Materials Society, 1984.
Gangloff RP. Hydrogen assisted cracking of high strength alloys. In: Milne I, Ritchie RO, Karihaloo B, editors-in-chief, Petit J, Scott P, volume editors. Comprehensive structural integrity, vol. 6. New York, NY: Elsevier Science, 2003: 31–101.
Gao M, Lu M, Wei RP. Crack paths and hydrogen-Afinssisted crack growth response in AlSi 4340 steel. Metall Trans A 1984; 15: 735–746.
Gates JD, Atrens A, Smith IO. Microstructure of as-quenched 3.5NiCrMoV rotor steel: I. General structure and retained austenite. Z Werkstofftech 1987; 18: 165–170.
Gerberich WW, Chen YT, St. John C. A short-time diffusion correlation for hydrogen-induced crack growth kinetics. Metall Trans A 1975; 6: 1485–1498.
Gerberich WW, Livne T, Chen X-F. In: Jones RH, Gerberich WW, editors. Modeling environmental effects on crack initiation and propagation. Warrendale, PA: The Minerals, Metals & Materials Society, 1986: 243–257.
Gerberich WW, Marsh PG, Hoehn JW. In: Thompson AW, Moody NR, editors. Hydrogen effects in materials. Warrendale, PA: The Minerals, Metals & Materials Society, 1996: 539–553.
Gibala R, DeMiglio DS. Hydrogen in iron and steels: Interactions, traps and crack paths. In: Hydrogen effects in metals. Warrendale, PA: Metallurgical Society of AIME, 1981: 113–122.
Grossbeck ML, Birnbaum HK. Low temperature hydrogen embrittlement of niobium. II. Microscopic observations. Acta Metall 1977; 25: 135–147.
Gutman EM. Notes on the discussion concerning the “surface mobility mechanism” of stress corrosion cracking. Corros Sci 2003; 45: 2105–2117.
Hall MM. An alternative to the Shoji crack tip strain rate equation. Corros Sci 2008; 50: 2902–2905.
Hall MM. Film rupture model for aqueous stress corrosion cracking under constant and variable stress intensity factor. Corros Sci 2009; 51: 225–233.
Hertzberg JL, Was GS. Isolation of carbon and grain boundary carbide effects on the creep and intergranular stress corrosion cracking behavior of Ni–16Cr–9Fe–xC alloys in 360°C primary water. Metall Mater Trans A 1998; 29: 1035–1046.

Hirose Y, Mura T. Growth mechanisms of stress corrosion cracking in high strength steels. Eng Fract Mech 1984; 19: 1057–1067.
Hirth JP. Adsorption at grain boundaries and its effect on decohesion. Philos Trans R Soc, A 1980a; 295: 139–149.
Hirth JP. Effects of hydrogen on the properties of iron and steel. Metall Trans A 1980b; 11: 861–890.
Hirth JP, Nix WD. Analysis of cavity nucleation in solids subjected to external and internal stresses. Acta Metall 1985; 33: 359–368.
Hirth JP, Rice JR. On the thermodynamics of adsorption at interfaces as it influences decohesion. Metall Trans A 1980; 11: 1501–1511.
Hoar TP, West JM. Mechano-chemical anodic dissolution of austenitic stainless steel in hot chloride solution. Proc R Soc A 1962; 268: 304–315.
Hodge JM, Mogford IL. UK experience of stress corrosion cracking in steam turbine discs. Proc – Inst Mech Eng 1979; 96: 193.
Issacs HS, Vyas B. Electrochemical corrosion testing. ASTM STP 727. American Society for Testing and Materials 1981: 3.
Jia JX, Song G, Atrens A. Experimental measurement and computer simulation of galvanic corrosion of magnesium coupled to steel. Adv Eng Mater 2007; 9: 65–74.
Jin L-Z. Chloride stress-corrosion cracking behavior of stainless steels under different test methods. J Mater Eng Perform 1994; 3: 734–739.
Johnson HH, Hirth JP. Internal hydrogen supersaturation produced by dislocation transport. Metall Trans A 1976; 7: 1543–1548.
Johnson HH, Lin RW. Hydrogen and deuterium trapping in iron. In: Hydrogen effects in metals. Warrendale, PA: Metallurgical Society of AIME, 1981: 3–25.
Jones RH. Stress corrosion cracking. Metals Park, OH: ASM International, 1992: 11.
Jung P. Compositional variation of hydrogen permeability in ferritic alloys and steels. J Nucl Mater 1996; 238: 189–197.
Kalderon D. Design of large steam turbines for fossil and nuclear power stations. Proc – Inst Mech Eng 1972; 186: 341.
Kerns GF, Wang MT, Staehle RW. Stress corrosion cracking and hydrogen embrittlement in high strength steels. In: Slater JE, editor. NACE-5 stress corrosion cracking and hydrogen embrittlement of iron base alloys. Houston, TX: NACE, 1977: 700–735.
Kinaev NN, Cousens DR, Atrens A. The crack tip strain field of AISI 4340. Part III. Hydrogen influence. J Mater Sci 1999; 34: 4931–4936.
Kortovich CS, Steigerwald EA. A comparison of hydrogen embrittlement and stress corrosion cracking in high-strength steels. Eng Fract Mech 1972; 4: 637–651.
Kumnick AJ, Johnson HH. Hydrogen transport through annealed and deformed Armco iron. Metall Trans 1974; 5: 1199–1206.
Kumnick AJ, Johnson HH. Deep trapping states for hydrogen in deformed iron. Acta Metall 1980; 28: 33–39.
Ladna B, Birnbaum HK. Study of hydrogen transport during plastic deformation. Acta Metall 1987; 35: 1775–1778.
Lea C. Met Sci 1980; 14: 107.
Lidbury DPG. In: Gangloff R.P. (editor), Embrittlement by the Localized Crack Environment. Warrendale, PA: Metallurgical Society of AIME, 1983: 149–172.
Lijie Q, Wuyang C, Huijun M, Jimei X, Peixin G. Hydrogen-facilitated corrosion and stress corrosion cracking of austenitic stainless steel of type 310. Metall Trans A 1993; 24: 959–962.
Liou H-Y, Shieh RI, Wei F-I, Wang S-C. Roles of microalloying elements in hydrogen induced cracking resistant property HSLA steel. Corrosion 1993; 49: 389–398.
Liu C, Macdonald DD. Prediction of failures of low-pressure steam turbine disks. J Pressure Vessel Technol 1997; 119: 393.
Liu Q, Irwanto B, Atrens A. The influence of hydrogen on 3.5NiCrMoV steel studied using the linearly increasing stress test. Corros Sci 2013; 67: 193–203.
Louthan MR Jr, McNitt RP, Sisson RD, editors. Environmental degradation of engineering materials in hydrogen. In: Proceedings of the 2nd International Conference on Environmental Degradation of Engineering Materials, 1981.
Lu Z, Shoji T. Unified interpretation of crack growth rates of Ni-base alloys in LWR environments. J Pressure Vessel Technol 2006; 128: 318–327.
Lufrano L, Sofronis P, Birnbaum HK. Elastoplastically accommodated hydride formation and embrittlement. J Mech Phys Solids 1998; 46: 1497–1520.
Lyle FF, Burghard HC. Mater Perform 1982; 35–44.
Lynch S. Hydrogen embrittlement phenomena and mechanisms. Corros Rev 2012a; 30: 105–123.
Lynch S. Mechanistic and fractographic aspects of stress corrosion cracking. Corros Rev 2012b; 30: 63–104.
Lynch SP. In: Swann PR, Ford FP, Westwood ARC, editors. Mechanisms of environment sensitive fracture of materials. London, UK: The Metals Society, 1977: 201–212.
Lynch SP. Mechanisms of hydrogen-assisted cracking. Met Forum 1979; 2: 189–200.
Lynch SP. Environmentally assisted cracking: Overview of evidence for an adsorption-induced localized slip process. Acta Metall 1988; 36: 2639–2661.
Lynch SP. In: Magnin T, editor. Second International Conference on Corrosion-Deformation Interactions. London, UK: The Institute of Materials, 1997: 206–219.
Lynch SP. Mechanisms of hydrogen assisted cracking – A review. In: International conference on hydrogen effects on material behaviour and corrosion deformation interactions. 2003: 449–466.
Lynch SP. Progress towards understanding mechanisms of hydrogen embrittlement and stress corrosion cracking. In: NACE – International corrosion conference series. 2007: 074931–0749355.
Maeng WY, Lee JH, Kim UC. Environmental effects on the stress corrosion cracking susceptibility of 3.5NiCrMoV steels in high temperature water. Corros Sci 2005; 47: 1876–1895.
Magdowski RM. In: Uggowitzer PJ, editor. Moderne Stahle. Zurich, 1987a: 107–140.
Magdowski RM. Stress corrosion cracking of low alloy steel in water. D Tech Sci thesis, Swiss Federal Institute of Technology, Zurich, 1987b.
Magdowski RM, Speidel MO. Clean steels for steam turbine rotors – their stress corrosion cracking resistance. Metall Trans A 1988; 19: 1583–1596.
Maiya PS, Shack WJ. In: Gangloff RP, editor. Effects of nominal and crack-tip strain rate on IGSCC susceptibility in CERT tests. In: Embrittlement by the localized crack environment. Warrendale, PA: Metallurgical Society of AIME, 1984: 199–209.
Maiya PS, Shack WJ. In: Gangloff RP, editor. Embrittlement by the localized crack environment. Warrendale, PA: Metallurgical Society of AIME, 1983: 199–209.
Maiya PS. Prediction of environmental and strain-rate effects on the stress corrosion cracking of austenitic stainless steels. J Pressure Vessel Technol 1987; 109: 116–123.

Marek M, Starke EA Jr. Potential distributions relating to grain boundaries on corroding aluminium alloys. Br Corros J 1976; 11: 31–34.
Marichev YA, Rosenfield IL. Corrosion 1976; 32: 423–429.
Mazzolai FM, Birnbaum HK. Elastic constant softening and short-range ordering phenomena in metal-hydrogen systems. J Phys Colloq 1985; 46: 81.
Mazzolai FM, Lewis FA. Elastic energy dissipation in the palladium-silver-hydrogen(deuterium) system. I. Hydrogen-dislocation interaction effects. J Phys F 1985; 15: 1249–1260.
McLean D, Northcott L. J Iron Steel Inst 1948; 158:169.
Nagumo M, Nakamura M, Takai K. Hydrogen thermal desorption relevant to delayed-fracture susceptibility of high-strength steels. Metall Mater Trans A 2001; 32: 339–347.
Nakayama T. Stress corrosion cracking of carbon steels and low alloy steels. Weld Int 2007; 21: 89–94.
Nelson HG, Williams DP. Quantitative observations of hydrogen induced slow crack growth in low alloy steel. In: Slater JE, editor. NACE-5 stress corrosion cracking and hydrogen embrittlement of iron base alloys. Houston, TX: NACE, 1977: 390–404.
Newman JF. The stress corrosion of steel in sodium hydroxide solution: A film-rupture model. Corros Sci 1981; 21: 487–503.
Oehlert A, Atrens A. Overview No 114: Room temperature creep of high strength steels. Acta Metall Mater 1994; 42: 1493–1508.
Oehlert A, Atrens A. The initiation and propagation of stress corrosion cracking in AISI 4340 and 3.5 Ni-Cr-Mo-V rotor steel in constant load tests. Corros Sci 1996; 38: 1159–1169.
Oehlert A, Atrens A. Stress corrosion crack propagation in AerMet 100. J Mater Sci 1998; 33: 775–781.
Oriani RA. The diffusion and trapping of hydrogen in steel. Acta Metall 1970; 18: 147–157.
Oriani RA. The mechanistic theory of hydrogen embrittlement of steels. Ber Bunsen-Ges 1972; 76: 848–857.
Oriani RA. Hydrogen embrittlement of steels. Annu Rev Mater Sci 1978; 8: 327–357.
Oriani RA. Hydrogen – The versatile embrittler. Corrosion 1987; 43: 390–397.
Oriani RA, Josephic PH. Equilibrium aspects of hydrogen-induced cracking of steels. Acta Metall 1974; 22: 1065–1074.
Oriani RA, Josephic PH. Equilibrium and kinetic studies of the hydrogen-assisted cracking of steel. Acta Metall 1977; 25: 979–988.
Oriani RA, Josephic PH. Effects of hydrogen on the plastic properties of medium-carbon steels. Metall Trans A 1980; 11: 1809–1820.
Padmanabhan R, Wood WE. Hydrogen induced cracking in a low alloy steel. Metall Trans A 1983; 14: 2347.
Page RA, Gerberich WW. The effect of hydrogen source on crack initiation in 4340 steel, Metall Trans A 1982; 13: 305–311.
Parker JG. Initiation of stress corrosion cracks in a low alloy steel. Br Corros J 1973; 8: 124–127.
Parkins RN. Stress corrosion spectrum. Br Corros J 1972; 7: 15–28.
Parkins RN. The controlling parameters of stress corrosion cracking. In: 5th Symposium on Line Pipe Research. Houston, TX: American Gas Institute, 1974.
Parkins RN. Development of strain rate testing and its implications. In: Stress corrosion cracking: The slow strain rate technique, ASTM STP 665. 1979a: 5–25.
Parkins RN. Stress corrosion cracking of ferritic steels. In: Parkins RN, editor. Stress corrosion research. Netherlands: Sijthoff and Noordoff, 1979b: 29–64.
Parkins RN. Strain rate effects in stress corrosion cracking. Corrosion 1990; 46: 178–189.
Parkins RN, Belhimer E, Blanchard WK. Stress corrosion cracking characteristics of a range of pipeline steels in carbonate-bicarbonate solution. Corrosion 1993; 49: 951–966.
Peisl H. Lattice strains due to hydrogen in metals. Hydrogen Met I 1978; 74: 53–74.
Pendley M. Sulfide stress cracking in steels – A review. In: Proceedings AIST Steel Properties and Applications. Mater Sci Technol 2010. 2010; 189–196.
Pérez Escobar D, Duprez L, Atrens A, Verbeken K. Thermal desorption spectroscopy study of experimental Ti/S containing steels. Mater Sci Technol, doi: 10.1179/1743284712Y.0000000141.
Pérez Escobar D, Minambres C, Duprez L, Verbeken K, Verhaege M. Internal and surface damage of multiphase steels and pure iron after electrochemical hydrogen charging. Corros Sci 2011; 53: 3166–3176.
Pérez Escobar D, Wallaert E, Duprez L, Atrens A, Verbeken K. Thermal desorption spectroscopy study of the interaction of hydrogen with TiC precipitates. Met Mater Int, doi: 10.1007/s12540-013-4013-7.
Petch NJ. Lowering of fracture-stress due to surface adsorption. Philos Mag 1956; 1: 331–337.
Pressouyre GM, Bernstein IM. A quantitative analysis of hydrogen trapping. Metall Trans A 1978; 9: 1571–1580.
Ramamurthy S, Atrens A. The stress corrosion cracking of as-quenched 4340 and 3.5NiCrMoV steels under stress rate control in distilled water at 90°C. Corros Sci 1993; 34: 1385–1402.
Ramamurthy S, Atrens A. The influence of applied stress rate on the SCC of 4340 and 3.5 NiCrMoV steels in distilled water 30°C. Corros Sci 2010; 52: 1042–1051.
Ramamurthy S, Lau WML, Atrens A. Influence of the applied stress rate on the stress corrosion cracking of 4340 and 3.5NiCrMoV steels under conditions of cathodic hydrogen charging. Corros Sci 2011; 53: 2419–2429.
Rebak RB. Industrial experience on the caustic cracking of stainless steels and nickel alloys – A review. In: Corrosion 2006, NACE – International Corrosion Conference Series. 2006: 065011–0650116.
Rebak RB, Xia Z, Szklarska-Smialowska Z. Effects of carbides on susceptibility of alloy 600 to stress corrosion cracking in high-temperature water. Corrosion 1993; 49: 867–876.
Rhodes PR. Environment-assisted cracking of corrosion-resistant alloys in oil and gas production environments: A review. Corrosion 2001; 57: 923–966.
Rieck RM. The mechanism of stress corrosion cracking of quenched and tempered low alloys steels in water. PhD thesis, University of Queensland, Australia, 1985.
Rieck RM, Atrens A, Ramamurthy S, Gates JD, Smith IO. In: International Conference on Environment Induced Cracking, October 1988, Kohler, WI, USA.
Rieck RM, Atrens A, Smith IO. The role of crack tip strain rate in the stress corrosion cracking of high strength steels in water. Metall Trans A 1989; 20: 889–895.
Rieck RM, Atrens A, Ramamurthy S, Gates JD, Smith IO. Conceptual model of stress corrosion cracking of low-alloy steels in high-temperature water. In: Gangloff RP, Ives MB, editors. Proceedings of the First International Conference on

Environment-Induced Cracking of Metals. Houston, TX: NACE, 1990.
Robertson JM, Birnbaum HK. An HVEM study of hydrogen effects on the deformation and fracture of nickel. Acta Metall 1986; 34: 353–366.
Rozenak P. Hydrogen effects on the behaviour of dislocations in austenitic stainless steel. J Mater Sci Lett 1990; 9: 627–629.
Salmond J, Atrens A. SCC of copper using the linearly increasing stress test. Scr Metall Mater 1992; 26: 1447–1450.
Sandoz G. A unified theory for some effects of hydrogen source, alloying elements, and potential on crack growth in martensitic AISI 4340 steel. Metall Trans 1972; 3: 1169–1176.
Scully JC. Kinetic features of stress-corrosion cracking. Corros Sci 1967; 7: 197–207.
Scully JC. The current situation in stress corrosion studies. Met Sci 1972a; 6: 238–240.
Scully JC. The theory of stress corrosion cracking in alloys. NATO, 1972b: 1–471.
Scully JC. Stress corrosion crack propagation: A constant charge criterion. Corros Sci 1975; 15: 207–224.
Scully JC. Mechanism of dissolution-controlled cracking. Met Sci 1978; 12: 290–300.
Scully JC. The interaction of strain-rate and repassivation rate in stress corrosion crack propagation. Corros Sci 1980; 20: 997–1016.
Scully JR, Van Den Avyle JA, Cieslak MJ, Romig AD, Hills CR. The influence of Pd on the hydrogen-assisted cracking resistance of PH 13-8 Mo stainless steel. Metall Trans A 1991; 22: 2429–2443.
Serebrinsky SA, Duffo GS, Galvele JR. Effect of strain rate on stress corrosion crack velocity: difference between intergranular and transgranular cracking. Corros Sci 1999; 41: 191–195.
Shih DS, Robertson LM, Birnbaum HK. Hydrogen embrittlement of α titanium: In situ TEM studies. Acta Metall 1988; 36: 111–124.
Sieradzki K, Friedersdorf F. Notes on the surface mobility mechanism of stress-corrosion cracking. Corros Sci 1994; 36: 669–675.
Sieradzki K, Newman RC. Brittle behaviour of ductile metals during stress-corrosion cracking. Philos Mag A 1985; 51: 95–132.
Simmons GW, Pao PS, Wei RP. Fracture mechanics and surface chemistry studies of subcritical crack growth in AISI 434o steel. Metall Trans A 1978; 9: 1147–1158.
Speidel MO. In: Speidel MO, Atrens A, editors. Proceedings corrosion in power generating equipment. New York: Plenum, 1984: 85–130.
Speidel MO, Bertilsson JE. Stress corrosion cracking of steam turbine rotors. In: Speidel MO, Atrens A, editors. Corrosion in power generating equipment. 1984: 331–357.
Speidel MO, Magdowski RM. In: Robert JTA, Weeks JR, Theus G, editors. Stress corrosion cracking of steam turbine steels – An overview. Proceedings of the Second International Symposium on Environmental Degradation of Materials in Nuclear Power Systems – Water Reactors. La Grange Park, IL: American Nuclear Society, 1986: 267–275.
Staehle RW. Current understanding of film rupture model of stress corrosion cracking. Corrosion 1972; 28: 470–471.
Stevens MF, Bernstein IM. The role of aging reactions in the hydrogen embrittlement susceptibility of an HSLA steel. Metall Trans A 1985; 16: 1879–1886.
Takano S, Suzuki T. An electron-optical study of β-hydride and hydrogen embrittlement of vanadium. Acta Metall 1974; 22: 265–274.
Thomas RLS, Scully JR, Gangloff RP. Internal hydrogen embrittlement of ultrahigh-strength AerMet®100 Steel. Metall Trans A 2003; 34: 327–344.
Thompson AW, Bernstein IM. Microstructure and hydrogen embrittlement. In: Bernstein IM, editor. Hydrogen effects in metals. Warrendale, PA: Metallurgical Society of AIME, 1981: 291–308.
Tien JK, Thompson AW, Bernstein IM, Richards RJ. Hydrogen transport by dislocations. Metall Trans A 1976; 7: 821–829.
Tien JK, Nair SV, Jensen RR. Dislocation sweeping of hydrogen and hydrogen embrittlement. In: Hydrogen effects in metals. Warrendale, PA: Metallurgical Society of AIME, 1981: 37–56.
Toloczko MB, Andresen PL, Bruemmer SM. SCC crack growth of cold-worked type 316 SS in simulated BWR oxidizing and hydrogen water chemistry conditions. In: Proceedings of the 13th International Conference on Environmental Degradation of Materials in Nuclear Power Systems. Toronto, Canada: Canadian Nuclear Society, 2007: 1672–1683.
Troiano AR. Embrittlement by hydrogen and other interstitials. Met Prog 1960; 77: 112–117.
Turnbull A. Test methods for environment assisted cracking. Br Corros J 1992; 27: 271–89.
Turnbull A. Modelling of environment assisted cracking. Corros Sci 1993; 34: 921–960.
Vermilyea DA. A film rupture model for stress corrosion crack propagation. Corrosion 1972; 28: 471.
Vermilyea DA. In: Staehle RW, Hochmann J, McCright RD, Slater JE, editors. Stress-corrosion cracking and hydrogen embrittlement of iron-base alloys. Houston, TX: NACE, 1977: 208–217.
Vermilyea DA, Diegle RB. Concerning strain-enhanced mechanisms of stress corrosion cracking. Corrosion 1976; 32: 26–29.
Villalba E, Atrens A. An evaluation of steels subjected to rock bolt SCC conditions. Eng Failure Anal 2007; 14: 1351–1393.
Villalba E, Atrens A. SCC of commercial steels exposed to high hydrogen fugacity. Eng Failure Anal 2008a; 15: 617.
Villalba E, Atrens A. Metallurgical aspects of rock bolt stress corrosion cracking. Mater Sci Eng A 2008b; 91: 8–18.
Vogt H, Speidel MO. Stress corrosion cracking of two aluminium alloys: A comparison between experimental observations and data based on modelling. Corros Sci 1998; 40: 251–270.
Wang J, Atrens A. Microstructure and grain boundary microanalysis of X70 pipeline steel. J Mater Sci 2003a; 38: 323–330.
Wang JQ, Atrens A. SCC initiation for X65 pipeline steel in the “high” pH carbonate/bicarbonate solution. Corros Sci 2003b; 45: 2199–2217.
Wang JQ, Atrens A. Analysis of service stress corrosion cracking in a natural gas transmission pipeline, active or dormant? Eng Failure Anal 2004; 11: 3–18.
Wang ZF, Atrens A. Initiation of stress corrosion cracking for pipeline steels in a carbonate-bicarbonate solution. Metall Mater Trans A 1996; 27: 2686–2691.
Wang JQ, Atrens A, Cousens DR, Kelly PM, Nockolds C, Bulcock S. Measurement of grain boundary composition for X52 pipeline steel. Acta Mater 1998; 46: 5677–5687.
Wang M, Akiyama E, Tsuzaki K. Effect of hydrogen on the fracture behavior of high strength steel during slow strain rate test. Corros Sci 2007; 49: 4081–4097.
Warke WR. Stress-corrosion cracking. In: Becker WT, Shipley RJ, editors. ASM handbook. Volume 11, Failure analysis and prevention. Metals Park, OH: ASM, 2002: 823–860.

Wert JA. Observations on hydrogen induced delayed plasticity and cracking in 4340 steel. Corrosion 1983; 39: 71–73.
Westlake DG. Generalized model for hydrogen embrittlement. ASM Trans Q 1969; 62: 1000–1006.
Winzer N, Atrens A, Dietzel W, Raja VS, Song G, Kainer KU. Characterisation of stress corrosion cracking (SCC) of Mg-Al alloys. Mater Sci Eng A 2008; 488: 339–351.
Winzer N, Atrens A, Dietzel W, Song G, Kainer KU. Comparison of the linearly increasing stress test and the constant extension rate test in the evaluation of transgranular stress corrosion cracking of magnesium. Mater Sci Eng A 2008; 472: 97–106.
Winzer N, Atrens A, Song G, Ghali E, Dietzel W, Kainer KU, Hort N, Blawert C. A critical review of the stress corrosion cracking (SCC) of magnesium alloys. Adv Eng Mater 2005; 7: 659–693.
Winzer N, Atrens A, Dietzel W, Song G, Kainer KU. Evaluation of the delayed hydride cracking mechanism for transgranular stress corrosion cracking of magnesium alloys. Mater Sci Eng A 2007; 466: 18–31.
Yamakawa K, Yonezawa S, Yoshizawa S. In: International Congress on Metallic Corrosion. Toronto, Canada: National Research Council, 1984: 254–261.
Yamamoto K, Ueno M, Higashiyama H, Sato T, Hashimoto M. Discussion on sulfide stress corrosion cracking test method. Houston, TX: NACE, 1985: 1–219.
Yoo CH, Lee HM, Chan JW, Morris JW. M2C precipitates in isothermal tempering of high Co-Ni secondary hardening steel. Metall Mater Trans, A 1996; 27: 3466–3472.
Yoshino Y. Metallurgical influences on the hydrogen uptake by steel in H_2S environments. Corrosion 1983; 39: 435–444.
Zakroczymski T, Szklarska-Smialowska Z. Activation of the iron surface to hydrogen absorption resulting from a long cathodic treatment in NaOH solution. J Electrochem Soc 1985; 132: 2548–2552.
Zapffe CA, Sims CE. Hydrogen, flakes and shatter cracks – Correlated abstract. Met Alloys 1940; 11: 177–184.
Zhang YP, Shi DM, Chu W, Qiao LJ, Shi YL, Zheng SL, Wang SB. Hydrogen-assisted cracking of T-250 maraging steel. Mater Sci Eng A 2007; 417: 34–37.

Sridhar Ramamurthy is a senior research scientist at Surface Science Western, a consulting and research laboratory specializing in the analysis and characterization of surfaces and materials at the University of Western Ontario, London, Ontario, Canada. Sridhar has over 20 years of experience in the application of surface analytical techniques to corrosion and electrochemical research. Currently, he is involved in a number of industry-sponsored research projects, such as the oxidation behavior of nickel-based alloys utilized in the nuclear industry, electrochemical behavior of materials for long-term nuclear waste storage, corrosion behavior of weathering steels, SCC of high-strength low-alloy steels and stainless steels, and electrochemical behavior of coated materials for automotive and food storage applications.

Andrej Atrens is professor of materials at The University of Queensland (UQ), where he has been since 1984. An international academic reputation is evident from invitations for keynote papers at international conferences (17 since 2001), invitations as guest scientist/visiting professor at leading international laboratories (in Belgium, Switzerland, Germany, France, and Sweden, 22 months since 2003), a high ISI H-index of 35 (web of science), many citations [5070 citations (web of science)], eight journal papers with more than 100 citations, six journal papers with more than 200 citations, and an excellent publication record in top international journals with more than 200 refereed journal publications. Research areas are SCC, corrosion of magnesium, corrosion mechanisms, atmospheric corrosion, and patination of copper.